

Article

Archaeometric Investigations on Archaeological Findings from Palazzo Corsini Alla Lungara (Rome)

Tilde de Caro ^{1,*} , Fiammetta Susanna ², Paola Fraiegarì ³, Renato Sebastiani ³, Veronica Romoli ⁴, Simone Bruno ⁵ and Andrea Macchia ⁶ 

¹ CNR ISMN, Strada Provinciale 35d 9, 00010 Rome, Italy

² Faculty of Cultural Heritage, Uninettuno, Corso Vittorio Emanuele II, 39-00186 Rome, Italy; fiammetta.susanna@uninettunouniversity.net

³ MiC SS-ABAP-RM, Piazza dei Cinquecento, 67-00185 Rome, Italy; fraiegaripaola@gmail.com (P.F.); renato.sebastiani@cultura.gov.it (R.S.)

⁴ Ass. Culturale Archivio Caffarelli APS-ETS, Via Bocca di Leone, 25-00187 Rome, Italy; veronicaromoli5@gmail.com

⁵ Deloitte NextHub S.r.l. S.B., Via Tortona 25, 20144 Milan, Italy; sibruno@deloitte.it

⁶ DIBEST, University of Calabria, Via Pietro Bucci, 87036 Arcavacata, Italy; andrea.macchia@unical.it

* Correspondence: tilde.decaro@cnr.it

Abstract: This study reports the analytical investigations on clayey and ceramic finds, characterised by high variability in terms of prime materials, with the aim to determine the role of this important ceramic production situated close to the city walls, fortuitously found during service excavations developed in the garden of Palazzo Corsini in Rome. The complexity of the finds led to the choices of appropriate methodologies and techniques suitable for defining the diagnostic elements of each find. Optical microscopy (OM) combined with micro-Raman (μ -Raman) spectroscopy, X-ray diffractometry (XRD), scanning electron microscopy with energy-dispersive X-ray spectroscopy (SEM/EDS), and differential thermal analysis (DTA) were used to analyse the nature and microstructure of the ceramic and burned clay that were found. In such a complicated setting, the objective of conducting chemical analyses is to provide clues to describe the various kinds of ceramics produced, the production and processing methods, and, as a result, the typology of the workshop.

Keywords: ceramic production; Roman technology; Palazzo Corsini



Citation: de Caro, T.; Susanna, F.; Fraiegarì, P.; Sebastiani, R.; Romoli, V.; Bruno, S.; Macchia, A. Archaeometric Investigations on Archaeological Findings from Palazzo Corsini Alla Lungara (Rome). *Ceramics* **2024**, *7*, 137–165. <https://doi.org/10.3390/ceramics7010010>

Academic Editor: Gilbert Fantozzi

Received: 27 December 2023

Revised: 20 January 2024

Accepted: 23 January 2024

Published: 30 January 2024



Copyright: © 2024 by the authors. Licensee MDPI, Basel, Switzerland. This article is an open access article distributed under the terms and conditions of the Creative Commons Attribution (CC BY) license (<https://creativecommons.org/licenses/by/4.0/>).

1. Introduction

1.1. Palazzo Corsini Alla Lungara and Cavallerizza Courtyard

During maintenance work in the part of the garden called the “Cavallerizza” of Palazzo Corsini, finds and remains of structures were found.

The historic Palazzo Corsini is a Renaissance palace with a large garden located on the Janiculum Hill, in the Trastevere area, between the slopes of the hill and close to the Tiber.

The renovations completed by the architect Ferdinando Fuga (1699–1782) gave the palace its current form, with the development of the internal garden, known as the “Cavallerizza”, which is separated from the rest of the garden with iron gates [1].

Since that time, no more improvements have been made to the palace; the focus was reduced to conservation efforts instead. The Italian government acquired Palazzo Corsini in 1883, and the regal Accademia dei Lincei moved its headquarters there.

Palazzo Corsini is enclosed by the Gianicolo walls and is located in the area between the Janiculum Hill to the west and the Tiber to the east [2]. The hilly sector surrounding this area is characterised by the presence of numerous springs, which flow from the Monte Mario–Gianicolo–Vatican ridge into the bank of the Tiber. Since many of them are no longer visible, their identification was possible through historical documentation, bibliographical sources, and archaeological investigations. The most notable springs mentioned in the

literature are Acqua Pia, Acqua Lancisiana, and Acque Corsiniane, which were canalised in the past to provide water to fountains, rich homes, and troughs [3]. The Corsini waters flowed in the area where the garden of Palazzo Corsini extended. The area where Palazzo Corsini is located had a predominantly rural character in the early twentieth century. During the Augustean period, urbanisation quickly changed this area, and many noble families occupied this area.

1.2. The Archaeological Area

Due to maintenance work in 2018, significant archaeological remains were discovered on the “Cavallerizza” side of the internal garden of Palazzo Corsini alla Lungara (Figure 1).



Figure 1. The archaeological area of Palazzo Corsini alla Lungara (credit to Veronica Romoli).

Ruins of ancient structures and numerous ceramic and metallic remnants were discovered in the area shown in the plan (Figure 2).

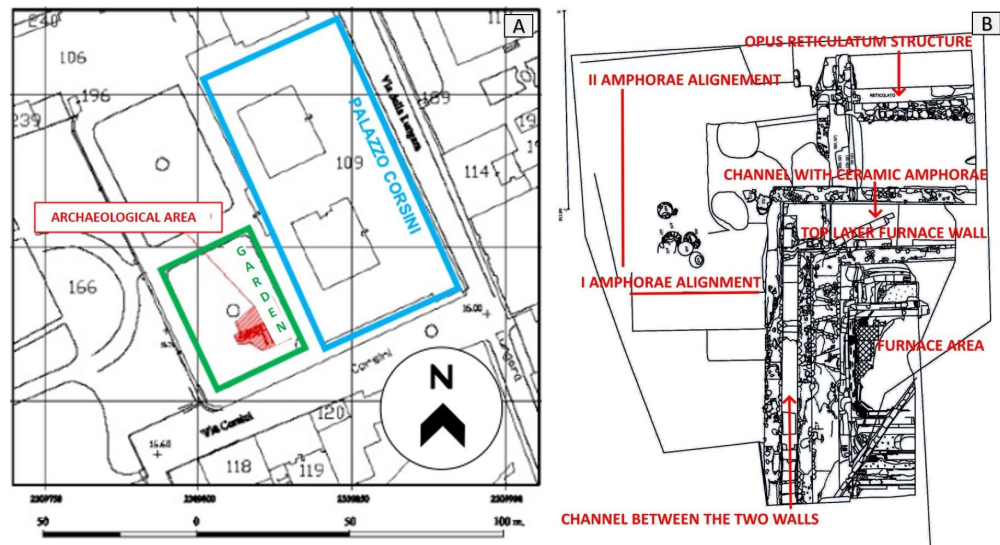


Figure 2. (A) Scale plan of the intervention area (red box) in the Cavallerizza courtyard (green) located in Palazzo Corsini alla Lungara (blue). (B) Detailed plan of the structures that emerged during the excavation (credit to Margherita Zannini).

The most notable finding was in the southern area, where a quadrangular-shaped clay floor cooked at high temperatures (backed clay) was discovered (Figure 3, area A).

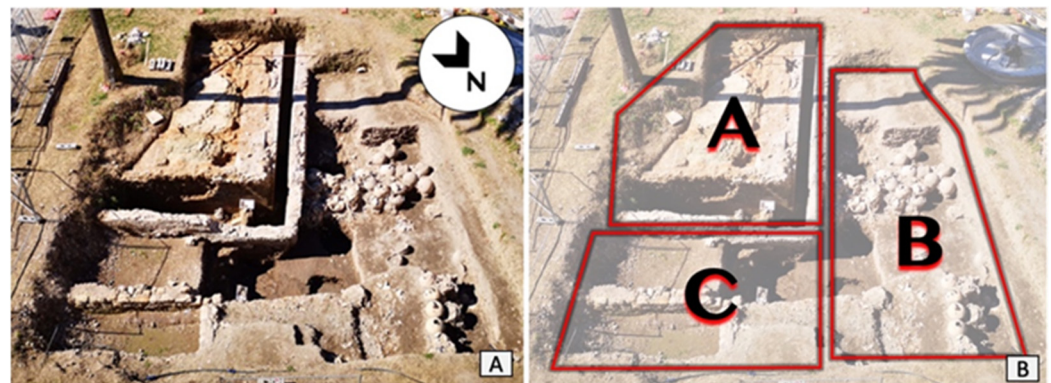


Figure 3. (A) Image of the archaeological excavation providing a general perspective of the structures discovered (credit to Veronica Romoli). The quadrants in (B) refer to the excavation areas where different materials and structures were found. Quadrant A indicates the area relating to the presumed furnace. Quadrant B indicates the area belonging to the location of the amphorae; Quadrant C indicates the area where there are walls of different eras.

Archaeologists think that the discovered structures are the remains of a manufacturing area. The quadrangular structure of the terracotta floor could indicate the presence of a cooking chamber of a furnace made up of a surface where the ceramic artefacts were placed and a vault that allowed the environment to be kept suitable by directing combustion gases outside, which was not found in our context [4].

Areas of distinct colours can be seen (Figure 4) in the surface layer of the backed clay floor (area A), which evidences the heating processes that produced the formation of various forms of oxidation in the components of the clay material.

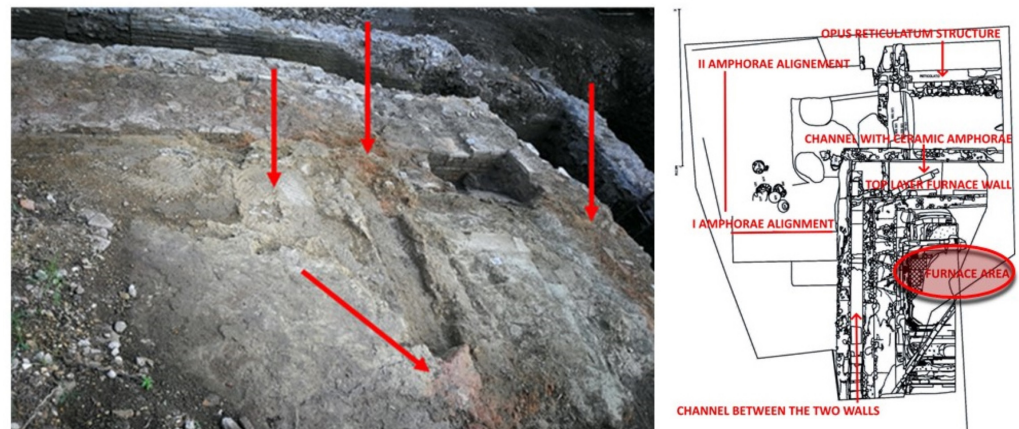


Figure 4. Areas with different colours (shown by arrows) may be visible in the surface layer of the backed clay floor (quadrant A, Figure 3B), indicating heating operations that resulted in the formation of various forms of oxidation in the clay material's components (credit to Veronica Romoli for the picture and to Margherita Zannini for the plant).

An extension of the excavation in the northern corner of the backed clay floor revealed a more elevated part of the same material (Figure 5). These materials could be the remains of the walls that could have supported the vault above the fireplace, the location of which has yet to be identified.



Figure 5. The remains of the walls (indicated by arrows) that could have supported the vault above the fireplace (credit to Veronica Romoli).

In the south-west sector of the area reported in quadrant A in Figure 3, two walls that could have been constructed later were discovered (Figure 6A).



Figure 6. (A) Walls of south-west sector of area A. (B) Canalisation formed between the two walls (credit to Veronica Romoli for the picture and to Margherita Zannini for the plant).

Another wall is settled frontally and parallel to it, a few centimetres apart (approximately 80 cm) from the other wall, providing a narrow passage (Figure 6B) comparable to a canal with a possible distribution or drainage function for water. This theory is supported by the presence of a multi-level floor that flows into a well and then into a cistern.

In addition to the succession of building phases, a significant number of the materials recovered during the excavation included ceramic artefacts, such as basin rims with sinusoidal handles, jugs, and planting pots, which are classified as common pottery and date from the I to III century AD. The stratigraphy of the sector between the two walls (quadrant C Figure 3) contains a variety of features, including friable and sandy earth with ceramic fragments on one side, pozzolanic earth on the other, and a portion of clayey and compact earth with a dark colour due to the presence of carbon. This part has a variety of precious objects, such as lamps, which are distinguished from the rest of the findings in the area by the presence of common pottery [5].

The wall to the east of the investigated site circumscribes a larger area, at the bottom of which is part of a mortar surface with a canal in the centre. This channel is filled with large cylindrical amphorae (Figure 7). The stratigraphy of the entire surrounding area is mainly

composed of a layer of ceramic fragments of various sizes, which could have a draining function.



Figure 7. Channel filled with ceramic amphorae from the 1st and 2nd centuries AD (credit to Veronica Romoli for the picture and to Margherita Zannini for the plant).

Two walls oriented perpendicularly may be seen covering the structure in the *opus reticulatum* in the north-east corner of the excavation (quadrant C) (Figure 8). The two perpendicular wall remains are made of burned clay blocks, some of which, archaeologists believe, came from the disintegration of the work surface. These walls appear to be the most recent phase of the investigation area.

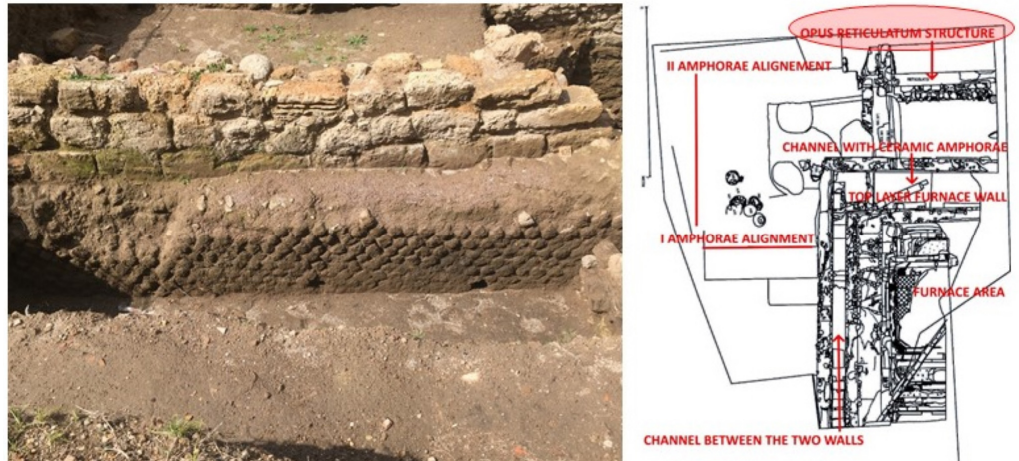


Figure 8. Post-ancient wall (wall above) and opus reticulatum structure (wall below) (credit to Veronica Romoli for the picture and to Margherita Zannini for the plant).

The discovered *opus reticulatum* wall structure can be dated between the first century BC and the first century AD [6]. This wall construction is not related to the reported production complex, but rather to an aristocratic villa, indicating a change in the intended use of the area from residential to work/productive purposes.

The stratigraphy of the sector between the two walls (quadrant C) contains a variety of features, including friable and sandy earth with ceramic fragments on one side, pozzolan earth on the other, and a portion of clayey and compact earth with a dark colour due to the presence of carbon. This part has a variety of precious objects, such as lamps, which are distinguished from the rest of the findings in the area by the presence of common pottery.

The excavations also led to the discovery of a double line of amphorae with east–west and north–west directions inside the excavated area (Figure 9).



Figure 9. The double line of Dressel 20-type oil amphorae (indicated by arrows) (credit to Veronica Romoli for the picture and to Margherita Zannini for the plant).

The placements of these amphorae in the excavation area indicate that they were positioned there to create a protective barrier to drain the water that came down from the Janiculum, which is an important function that kept the area dry. The amphorae were placed in a layer of very compact and extremely hard silty-clayey soil that appears to be rich in carbon, maybe from furnace waste or cleaning work on the furnace itself [7].

The discovered amphorae are mostly of the Dressel type. Dressel 20-type amphorae, attested from the Augustan age up to the second century AD [8], were used to contain the oil coming from the Roman province of Betica. This province, conquered by the Romans in 218 BC and located on the Iberian Peninsula, corresponding to the current Spanish region of Andalusia, was a large producer of olive oil and Betic oil, which were much appreciated by the Romans.

The objects found in the archaeological area include a considerable number of ceramic fragments and semi-finished bones.

Throughout the investigated area, numerous clay pieces were discovered with signs of green glassy frit, glassy slag, and places with high concentrations of minute glass pieces, indicating a phase of destruction or abandonment of the structure.

The findings discovered in the garden of the “Cavallerizza” of Palazzo Corsini were highly heterogeneous in terms of the materials and functions. They mainly included common furniture, attested in the Augustan age up to the first century AD, and common cooking tools attributed to the second half of the third century AD. In lesser quantities, there were also other types of materials, such as bronzes, bone carvings, and glass fragments.

1.3. The Structures of the “Cavallerizza” Courtyard: Furnace Hypothesis

Furnaces for ceramic production are classified according to their shapes (quadrangular or circular) [9], the division of the combustion chamber from the firing chamber, and the type of draught. The latter, with vertical draughts, also known as “vertical furnaces”, were the most common in Roman times and were very stable constructions that allowed the construction of large structures while avoiding heat dispersion and favouring a uniform frying of the materials [10–12].

The ceramic base discovered in the garden of Palazzo Corsini must belong to a quadrangular-shaped furnace. The combustion chamber is supposed to be located under the heating surface but has yet to be discovered in the current state of the works. The curbs on the baked clay floor most likely supported a vaulted roof, which was required to close the firing chamber. Furthermore, the absence of roof remains could suggest that it was destroyed after each firing cycle and rebuilt after the materials were repositioned on the perforated surface [13–15].

The structure found in the garden of Palazzo Corsini has a clay surface where different colours are highlighted, which vary from orange-red to blackish-grey (Figure 4), implying that it is a thermally transformed clay (hence the term baked clay). It may have been the ancient firing surface of the furnace, although, unlike the more common Roman furnaces, the heating surface is not perforated. Cuomo di Caprio [9] hypothesised that a temporary

perforated surface was likely utilised, i.e., formed and destroyed each time, to enable it to adapt more easily to large materials.

The furnace needed a large amount of water, which was essential for the control of fire and heat; the presence of a water channel around the floor could have been created not only as a function of channelling water resources, but also intentionally for the use of the furnace. The reason why this location was selected for the officina could be attributed to the presence of a clayey area, primarily composed of silty clays [16], which is suitable for the creation of artefacts, as well as the abundance of wood required for the kilns, whose supply was ensured by the proximity of the ports on the Tiber in the Trastevere area (port of Ripa Grande) and by the presence of numerous springs on the Janiculum that descended into the valley to flow into the Tiber. The region was thus in a particularly advantageous position for the supply of raw materials as well as for the transportation of finished products because of its close position to the river landings.

Although Palazzo Corsini's excavation remains incomplete, a number of indicators, including the presence of pigments, glass, bone, and metal fragments, point to the existence of an artisan complex that may have been used to produce ceramics as well as other materials.

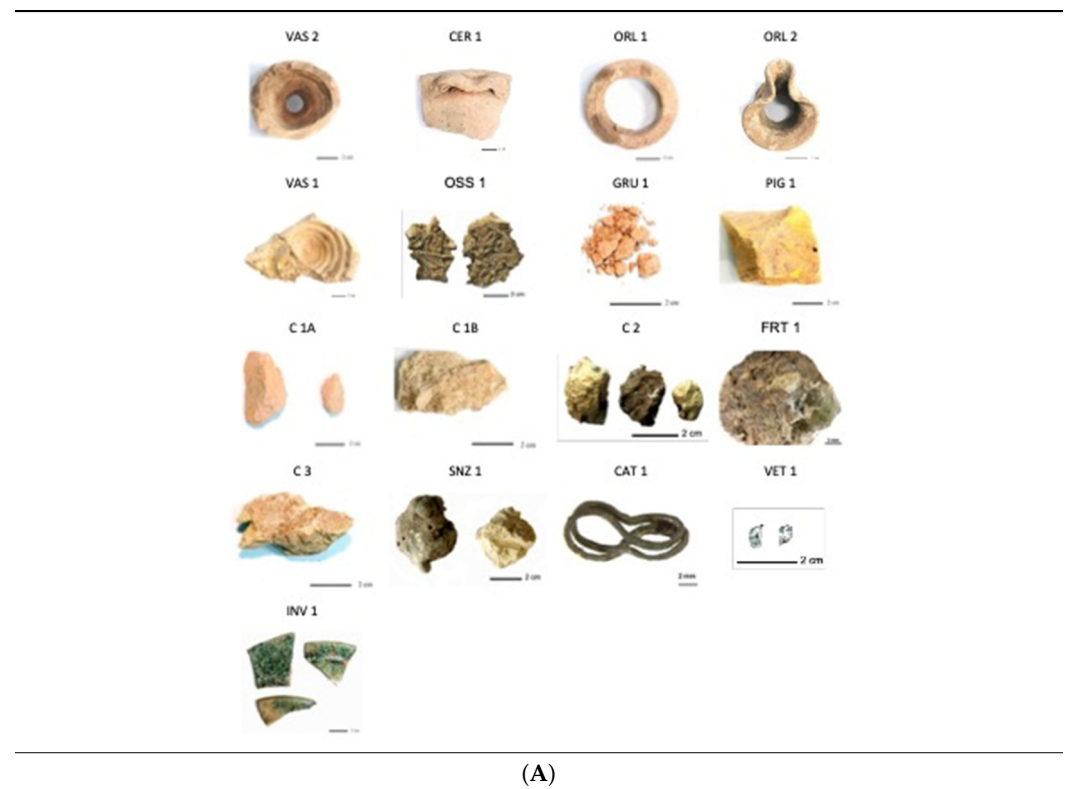
The goal of conducting chemical analyses in this sort of complex context is to offer indications that can help characterise the variety of ceramics produced, the methods used in their manufacturing and processing, and ultimately, the type of workshop situated so close to the city walls.

2. Materials and Methods

2.1. Materials

Sixteen findings, described in Table 1, representing the most significant categories of materials discovered during the archaeological excavation (such as ceramic artefacts, bones, and raw and burned clays), were subjected to chemical–physical investigations.

Table 1. Typology (A) and excavation reference of analysed materials (B).



(A)

Table 1. Cont.

Sample	Typology	Excavation reference
CER 1	Bowl fragment	US 99, area B
ORL 1	Neck of vessel	US 99, area C
ORL 2	Neck of vessel	US 99, area C
VAS 1	Bowl fragment with bone remains	US 99, area C
VAS 2	Base of vase	US 102, area C
INV 1	Glazed ceramic	US 17, area C
FRT 1	Frit	US 17, area B
GRU 1	Red clay	US 99, area B
PIG 1	Yellow clay	US 17 (M/3), area B
C 1A	Fired clay	Area A
C 1B	Fired clay	Area A
C2	Fired clay	Area A
C3	Fired clay	Area A
SNZ 1	Fired clay	?
VET 1	Shard of glass	Area C
OSS 1	Bone-processing remnant	US 99, area C

(B)

2.2. Analytical Methods

The materials were analysed by means of optical microscopy (OM), scanning electron microscopy (SEM), energy-dispersive X-ray spectroscopy (EDS), X-ray diffraction (XRD) analysis, micro-Raman (μ -Raman) spectroscopy, and thermogravimetric analysis (TGA). The analyses were carried out as follows:

- Optical microscopy (OM) investigations were performed using a Leica M125 C microscope equipped with a digital camera, Leica MC170 HD.
- Scanning electron microscopy with energy-dispersive X-ray spectroscopy (SEM/EDS) characterisations were carried out using a SEM TESCAN VEGA 3 equipped with a microprobe X-ray INCA 300 and a four-sector backscattered electron detector (BSE). The beam accelerating voltage was set between 20 and 30 keV, which was sufficient to overcome the critical energy of the electrons for the X-ray emission (quantitative resolution limit of 0.2% by weight) and working distance (WD) of 15 mm.
- The structural identification of crystalline phases of the patinas was determined using a SEIFERT D3003 Theta-theta diffractometer (XRD) and Cu-filtered Cu K α radiation ($\lambda = 1.5418$) with a beam size of 1 cm². Angular values in the range between 10 and 80° in additive mode, a step size of 0.05°, and a sampling time of 2 s were the experimental parameters used for data acquisition. X-ray diffraction pattern analysis was carried out using RUFF online database (<https://ruff.info> accessed on 16 February 2023) and the instrument library.
- Micro Raman (μ -Raman) analysis was performed at room temperature using a Renishaw RM2000 equipped with a Peltier-cooled charge-coupled device (CCD) camera, in conjunction with a Leica optical microscope with X10, X20, X50, and X100 objectives. Measurements were performed using the X50 objective (laser spot diameter of about 1 μ m) and the 514.5 nm excitation line of an Ar⁺ laser using the equipped density filter with a real output of 300 μ W. Raman analysis was carried out using RUFF online database (<https://ruff.info> accessed on 17 February 2023) and the GRAMS library.
- The TG curves were obtained using a Perkin-Elmer PC series TGA-7 thermogravimetric analyser in the temperature range of 25–1000 °C. The dynamic experiments were carried out in an air and nitrogen atmosphere with a flow rate of 80 mL min⁻¹ and a heating rate of 10 °C min⁻¹.

3. Results

3.1. Ceramic Artefacts

The ceramic artefacts that were analysed (CER1, ORL1, ORL2, VAS1, and VAS2) are mostly remains of commonly used vases from quadrants B and C, as seen in Figure 10B.

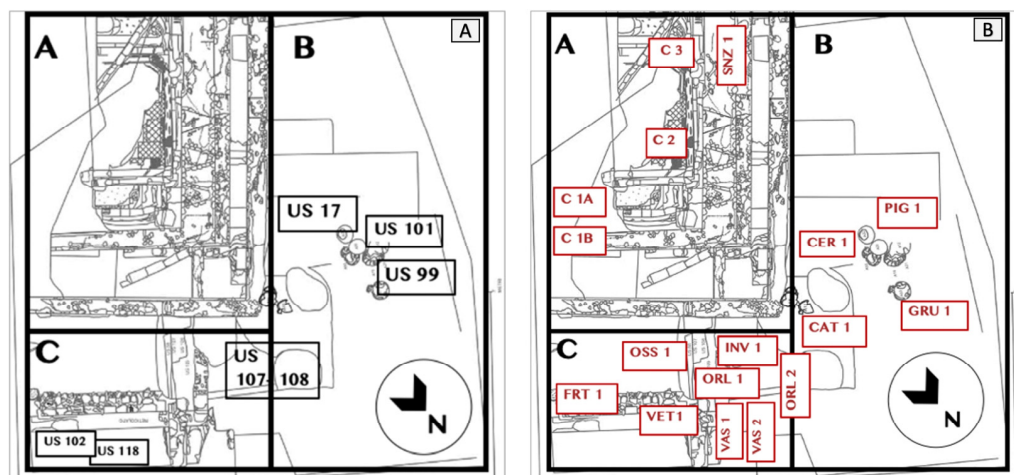


Figure 10. (A) Excavation plan with USS location for quadrants A, B, C and (B) location of the analysed materials (credit to Margherita Zannini).

During firing, solid-state reactions occur in the ceramic body under non-equilibrium conditions, leading to the nucleation and development of newly formed phases and, in some cases, compositional variations in the present phases. The identification of each phase allows us to hypothesise both the clay typology and the possible function of the artefact, as well as the manufacturing method and, thus, the technological level reached in the production workplace [17].

The observations in the optical and electronic microscopes of the bowl fragment CER 1 reveal that it has a homogenous morphology and a low porosity (Figure 11A,D). The EDS area analysis, carried out on the surface sample (Figure 11C, Table 2), revealed the presence of Si (20%), Ca (10.2%), and Al (7%) together with minor quantities of Fe, Na, Ti, and K. The XRD spectrum highlights the mineralogical phases present: quartz (SiO_2), calcite (CaCO_3), feldspar-albite ($\text{NaAlSi}_3\text{O}_8$), and gehlenite ($\text{Ca}_2\text{Al}(\text{AlSi})\text{O}_7$).

Table 2. EDS area analysis of vessel CER1; * weight per cent (wt%), error $\pm 0.2\%$.

	O	Na	Mg	Al	Si	K	Ca	Ti	Fe
<i>CER1</i> *	55.0	0.6	2.0	7.0	20.0	1.6	10.2	0.3	3.0

The thermogravimetric analysis (TG) (Figure 12) shows a point of flex between 700 °C and 900 °C, which is attributed to the decomposition of the calcite. The crystallisation temperature of gehlenite begins at $T > 800$ °C, and the presence of calcite, which dissociates between 700 °C and 800 °C, leads us to hypothesise that the furnace reached heating peaks of up to 900 °C, even if the average temperature was most likely lower.

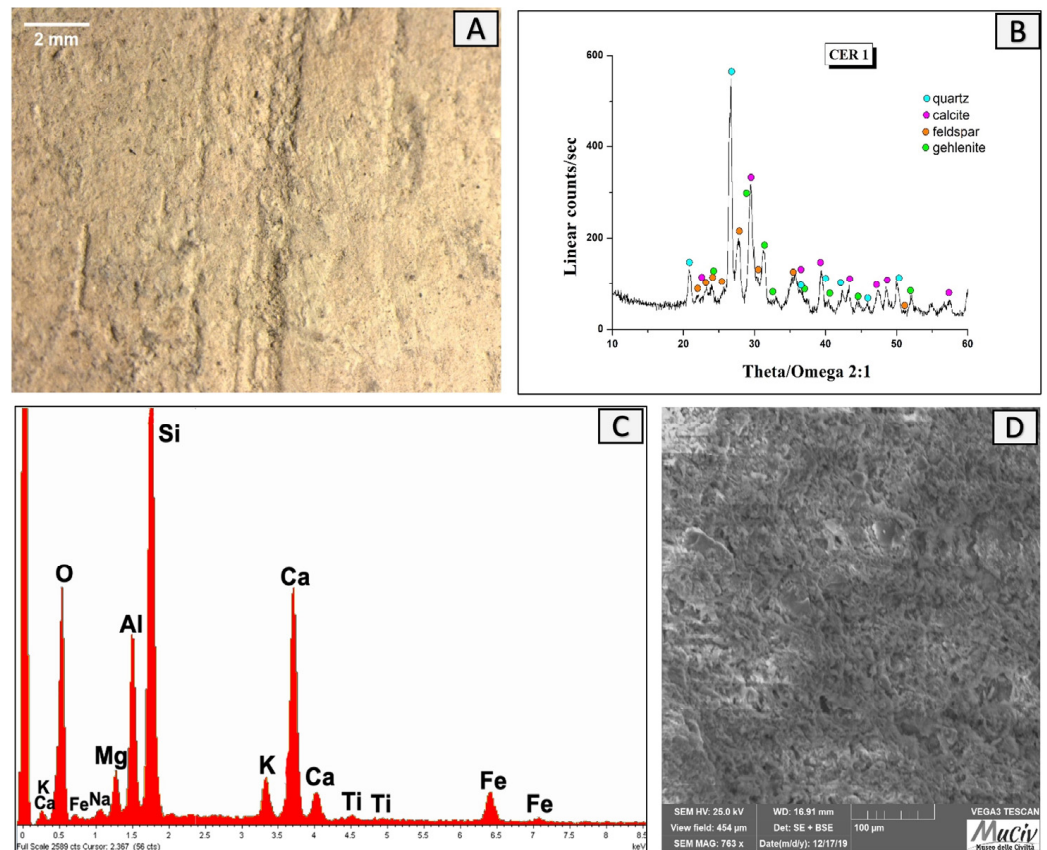


Figure 11. Surface analysis of the bowl fragment CER1. (A) Optical and (D) backscattered SEM images of ceramic surface. The XRD spectrum (B) reveals the mineralogical phases present: quartz (SiO_2), calcite (CaCO_3), feldspar-albite ($\text{NaAlSi}_3\text{O}_7$), and gehlenite ($\text{Ca}_2\text{Al}(\text{AlSi})\text{O}_7$). EDS area spectrum (C) reveals the presence of Si, Ca, and Al together with smaller quantities of Fe, Na, Ti, and K.

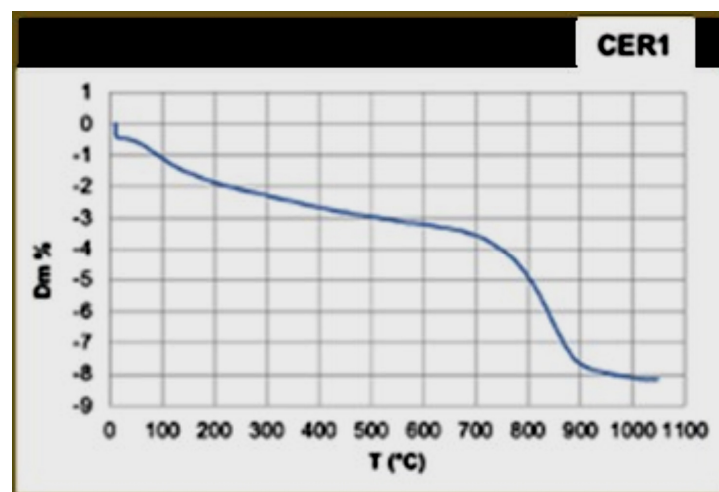


Figure 12. Thermogravimetric analysis (TG) of the CER1 basin shows a point of flex between 700 °C and 900 °C, which is attributed to the decomposition of the calcite.

In OM, the ORL 1 vessel's neck surface looked light in colour with a homogenous surface (Figure 13A). The SEM image (Figure 13D), acquired in backscattered electrons of a fragment section, disclosed a bubbled layer (denoted by the red box). The EDS area analyses (Figure 13C and Table 3) detected the presence of Si (11.0%), Ca (8.6%), Na (2.8%),

K (2.3%), and Al (1.6%), which are elements that suggest the possible presence of glass on the surface.

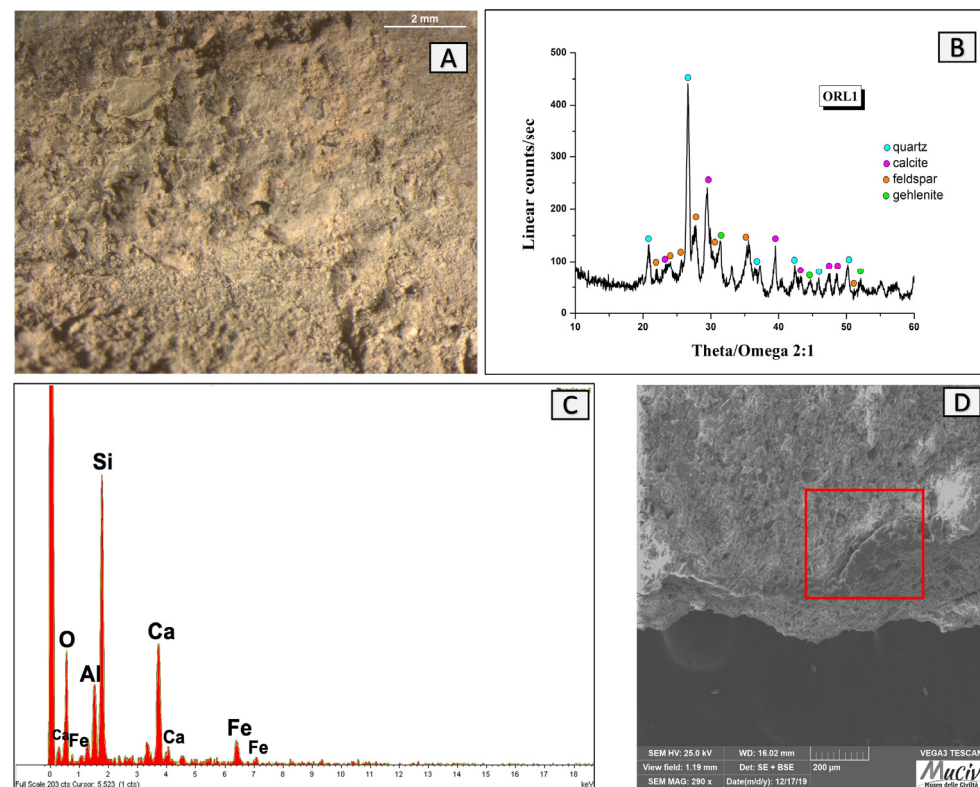


Figure 13. Surface analysis of glassy layer of neck of ORL1 vessel. (A) Optical and (D) backscattered SEM images of the vitrified surface of the ORL1 fragment (square in red). The XRD spectrum (B) reveals the mineralogical phases present: quartz (SiO_2), calcite (CaCO_3), albite ($\text{NaAlSi}_3\text{O}_8$), and gehlenite ($\text{Ca}_2\text{Al}(\text{AlSi})\text{O}_7$). The EDS spectrum (C) reveals the presence of Si, Ca, Na, K, and Al.

Table 3. EDS area analysis of ORL1 fragment; * weight per cent (wt%), error $\pm 0.2\%$.

	O	Na	Al	Si	Cl	K	Ca	Fe
ORL1 *	70	2.8	1.6	11.1	1.5	2.3	8.6	2.1

The mineral phases present in the glassy layer can be observed in the XRD spectrum (Figure 13B). The significant abundance of quartz (SiO_2) is linked to the probable presence of the glassy coating as well as the ceramic body. Quartz is found in association with the minerals calcite (CaCO_3), feldspar-albite ($\text{NaAlSi}_3\text{O}_8$), and gehlenite ($\text{Ca}_2\text{Al}(\text{AlSi})\text{O}_7$).

These characteristics are indicative of a transparent glass placed on the interior surface of the bowl, whose function was most likely to make the container waterproof to aid in the preservation of the food inside.

The OM and SEM images (Figure 14A,D) of the ORL 2 vessel's neck show a uniform ceramic matrix with a colour area changing from pinkish to greyish and a regular mixture. The colour variability could indicate a heating atmosphere that is not perfectly controlled, with a gradient of oxidising and reducing conditions, as well as differential corrosion between the different areas in relation to the product's position or a mixing of different clays [18].

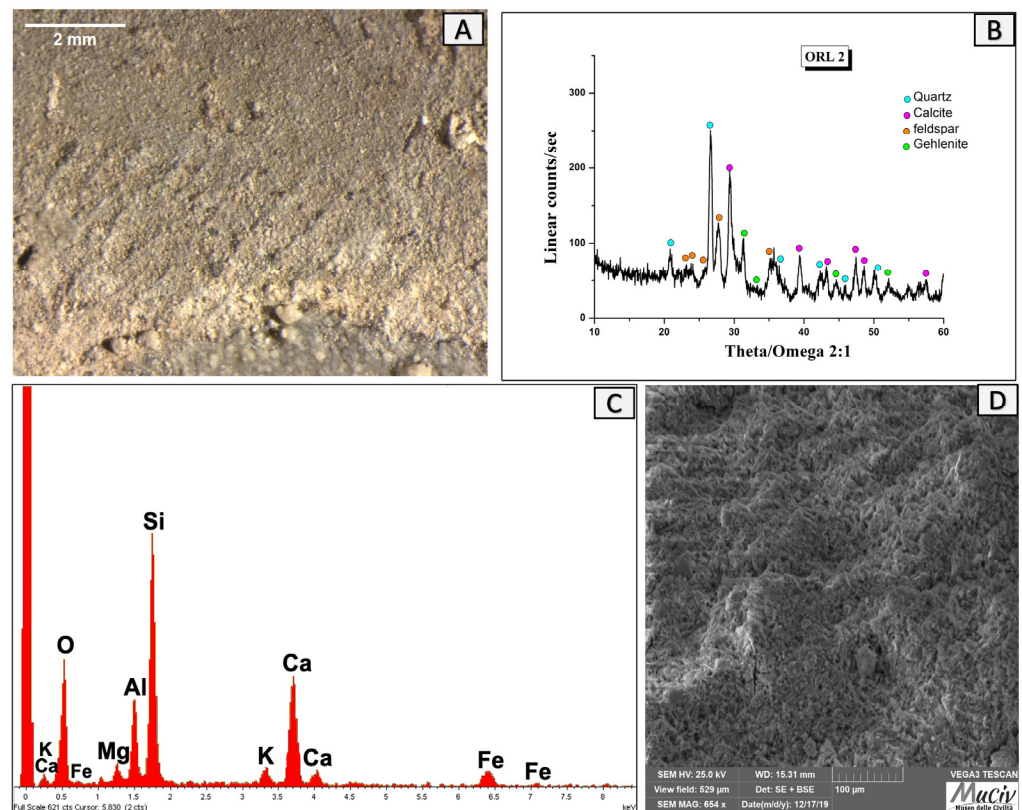


Figure 14. Surface analysis of neck of ORL2 vessel. (A) Optical and (D) backscattered SEM images of the ceramic surface. The XRD spectrum (B) reveals the presence of quartz (SiO_2), calcite (CaCO_3), albite ($\text{NaAlSi}_3\text{O}_8$), and gehlenite ($\text{Ca}_2\text{Al}(\text{AlSi})\text{O}_7$). The EDS area spectrum (C) reveals high concentrations of Si, Al, and Ca and reduced quantities of Fe and K.

The EDS area spectrum and chemical analysis (Figure 14C, Table 4) detected high concentrations of Si (18%), Al (13%), and Ca (10.3%) and minor quantities of Fe and K.

Table 4. EDS area analysis of ORL2 fragment; * weight percentage (wt%), error $\pm 0.2\%$.

	O	Mg	Al	Si	K	Ca	Fe
ORL2 *	52.2	1.7	13.3	18.6	1.3	10.3	2.5

The XRD analysis (Figure 14B) revealed the presence of quartz (SiO_2), calcite (CaCO_3), feldspar-albite ($\text{NaAlSi}_3\text{O}_8$), and gehlenite ($\text{Ca}_2\text{Al}(\text{AlSi})\text{O}_7$).

The thermogravimetric analysis highlights a weight loss in the material analysed between approximately 700°C and 900°C (Figure 15) due to the decomposition of CaCO_3 . The low weight loss in the initial section of the reported curve reveals a low presence of adsorbed water due to the waterproof property of the ceramic [19].

The OM image (Figure 16A) of the bowl fragment with bone remains (VAS 1) shows a ceramic item with a large grain size range. Figure 16B shows the XRD spectrum of the sample; the most sharp and intense peaks on the diffractogram are related to quartz (SiO_2), calcite (CaCO_3), feldspar-albite ($\text{NaAlSi}_3\text{O}_8$), and gehlenite ($\text{Ca}_2\text{Al}(\text{AlSi})\text{O}_7$).

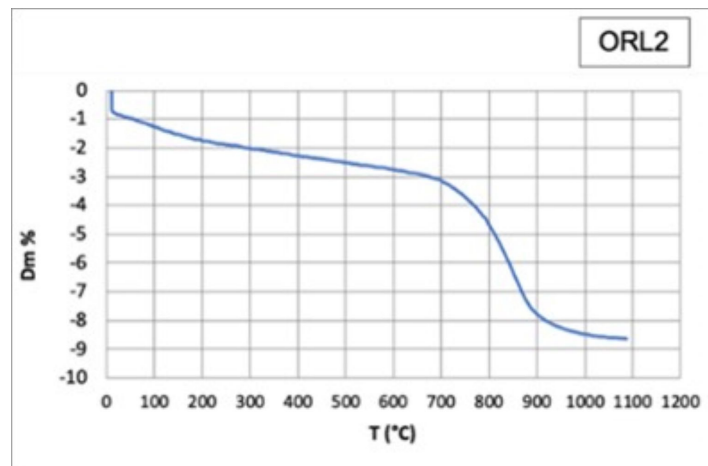


Figure 15. Thermogravimetric analysis (TG) of the ORL2 fragment shows a point of flex between 700 °C and 900 °C, which is attributed to the decomposition of the calcite.

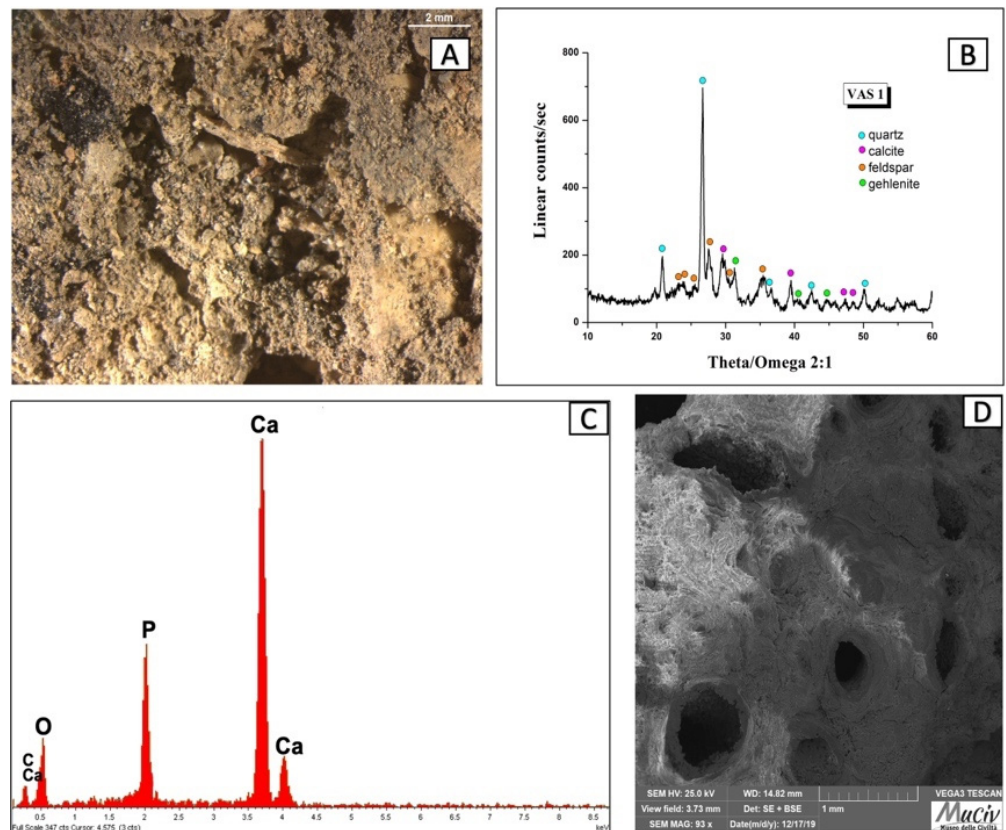


Figure 16. Surface analysis of the material attached to fragment of VAS1 vessel. (A) Optical and (D) backscattered SEM images (D) of the bottom remains. The XRD spectrum of the ceramic item (B) reveals the mineralogical phases present: quartz (SiO_2), calcite (CaCO_3), feldspar-albite ($\text{NaAlSi}_3\text{O}_8$), and gehlenite ($\text{Ca}_2\text{Al}(\text{AlSi})\text{O}_7$). The EDS spectrum (C) of the bottom remains reveals the presence of Ca and P due to the presence of hydroxyapatite, $\text{Ca}_{10}(\text{PO}_4)_6(\text{OH})_2$.

Figure 16C,D report the EDS area spectrum and the SEM image of the encrustation that is present on the bottom of the bowl. The SEM image identifies the structure of a bone material. The presence of Ca (26.4%) and P (9.5%), due to the presence of hydroxyapatite, $\text{Ca}_{10}(\text{PO}_4)_6(\text{OH})_2$, of which the bones are composed, is supported by the EDS area analysis (Figure 16C).

The image in OM of the base of VAS 2 vase (Figure 17A) indicates a structure composed by homogenous and light-coloured clay. The microcrystalline structure is visible in the SEM image (Figure 17D). The EDS area spectrum (Figure 17C) and the EDS area analyses (Table 5) highlight a homogeneous structure composed mainly of Si (23%), Al (7.3%), and Ca (6.2%). The μ -Raman spectra (Figure 17B) reveal the presence of goethite (FeO(OH)) and hematite (Fe₂O₃).

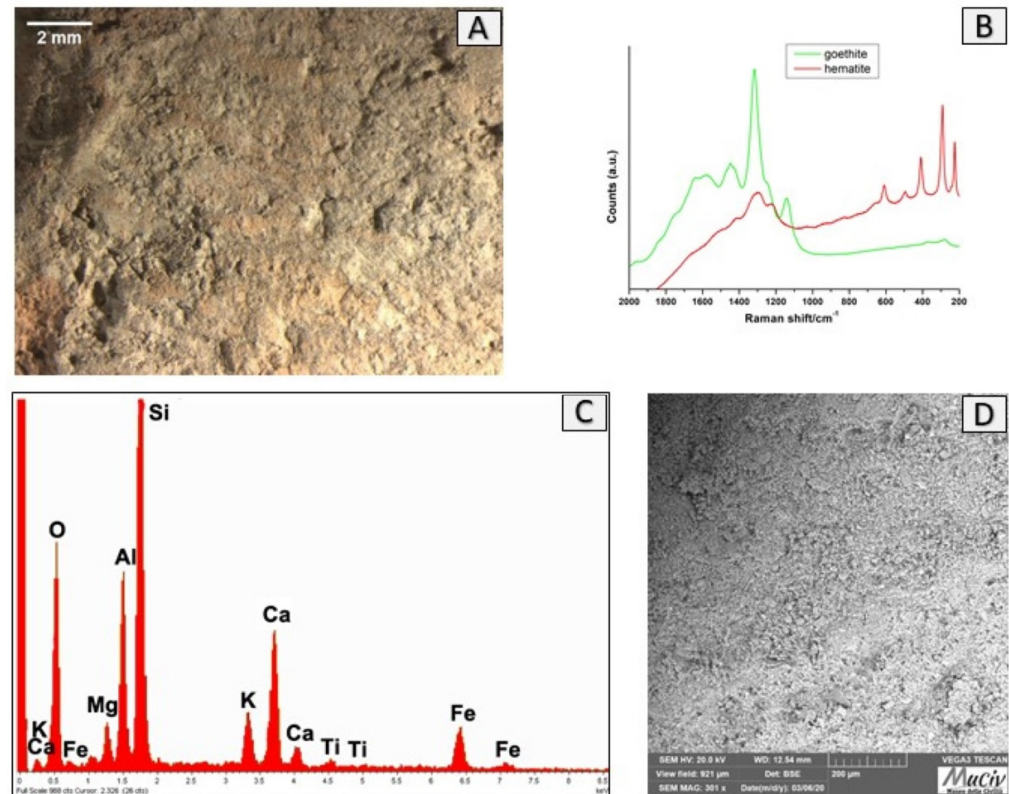


Figure 17. Surface analysis of the base of VAS2 vessel. (A) Optical and (D) backscattered SEM images of the ceramic surface. The μ -Raman spectra (B) reveal the presence of goethite (FeO(OH)) and hematite (Fe₂O₃). The EDS spectrum (C) highlights the presence of Si, Al, and Ca and smaller quantities of Fe, K, Mg, and Ti.

Table 5. EDS area analysis of the VAS2 fragment; * weight per cent (wt%), error \pm 0.2%.

	O	Mg	Al	Si	K	Ca	Ti	Fe
VAS2 *	50.2	2	7.3	23	2.7	6.2	0.3	8

The purity of the mixture and the morphology of the material suggest that it is a very fine ceramic.

3.2. Raw and Burned Clays

Numerous clay materials with a variety of colours and grain sizes were discovered during the archaeological excavation, some of which show evidence of combustion or thermal transformation that are commonly referred to as “burned clays.” These clays were most likely part of the structural works discovered during the excavation [20]. The materials analysed are from the quadrants A (C1A, C1B, C2, C3, and SNZ1) and B (GRU1 and PIG1).

The GRU1 clay (Figure 18A) has a coarse granulometry and a red-orange colour tone. The mineralogical analysis (Figure 18B) reveals the presence of quartz (SiO₂), calcite (CaCO₃), and albite-feldspar (NaAlSiO₃). The EDS area spectrum (Figure 18C) and chemical

area analyses (Table 6) show high concentrations of Si (18.2%), Fe (9.2%), and Ca (10.2%) and low contents of Al and Mg. The SEM images (Figure 18D) highlight a heterogeneous morphology in composition without evident forms of crystallisation and cohesion.

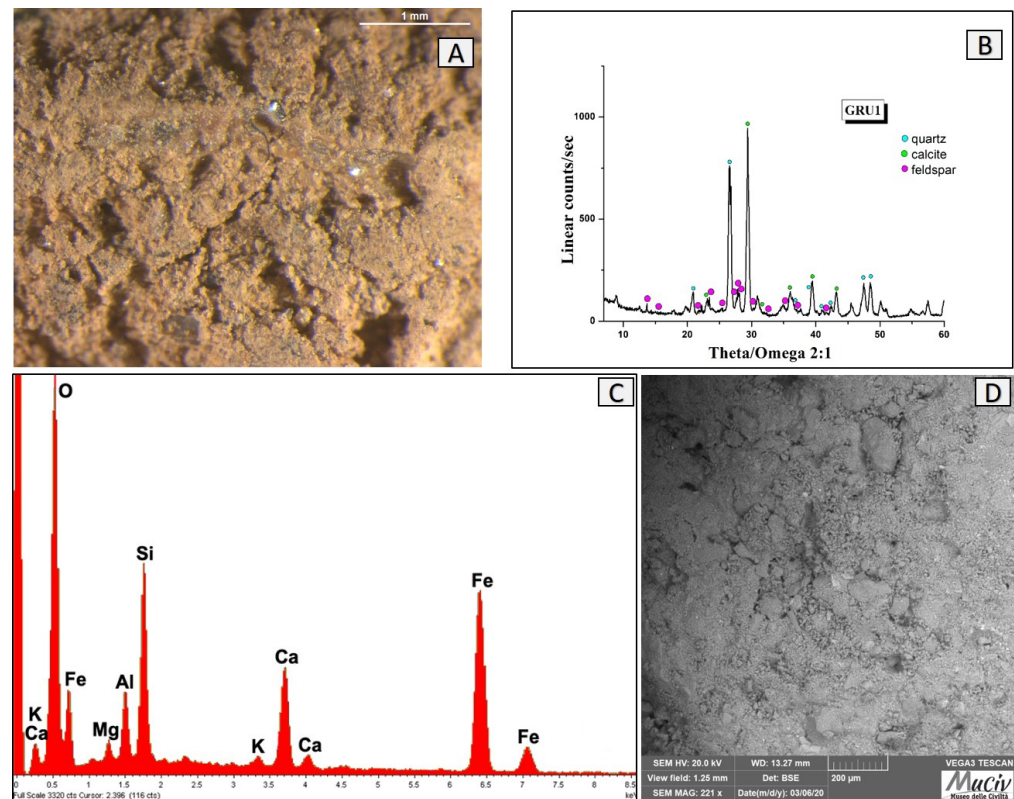


Figure 18. Surface area analysis of red clay GRU1. (A) Optical and (D) backscattered SEM images of the clay. The XRD spectrum (B) reveals the mineralogical phases present: quartz (SiO_2), calcite (CaCO_3), and albite-feldspar ($\text{NaAlSi}_3\text{O}_8$). The EDS area spectrum (C) reveals the presence of Si, Fe, and Ca and low contents of Al and Mg.

Table 6. EDS area analysis of the GRU1 red clay; * weight per cent (wt%), error $\pm 0.2\%$.

	O	Mg	Al	Si	K	Ca	Fe
<i>GRU1</i> *	55.8	1.2	4.1	18.2	1.1	10.2	9.2

The minerals that are present, including $(\text{Mg,Fe})\text{SiO}_3$, low-temperature feldspars (albite), quartz, and calcite, are typical of clay that has been subjected to a moderate thermal increase [21].

This clay fragment, found in a marginal area of the furnace and which shows no working traces, was probably part of a structure that was not subject to continuous heating.

The yellow PIG1 clay was discovered far from the furnace in the same area of the GRU1 clay. The OM image (Figure 19A) allows us to distinguish a uniform yellow ochre-coloured mixture with a very fine grain size, suggesting that it is a clay pigment. The XRD spectrum (Figure 19B) identifies calcite (CaCO_3), quartz (SiO_2), and goethite ($\text{FeO}(\text{OH})$). The μ -Raman analysis (Figure 19E) highlights the presence of limonite ($\text{FeO}(\text{OH}) \cdot n\text{H}_2\text{O}$). The SEM image, acquired with backscattered electrons (Figure 19D), shows a microcrystalline structure with one-dimensional and uniformly distributed crystals. The EDS area spectrum and chemical area analyses (Figure 19C, Table 7) reveal the presence of Ca (37.4%), Fe (6.7%), and Si.

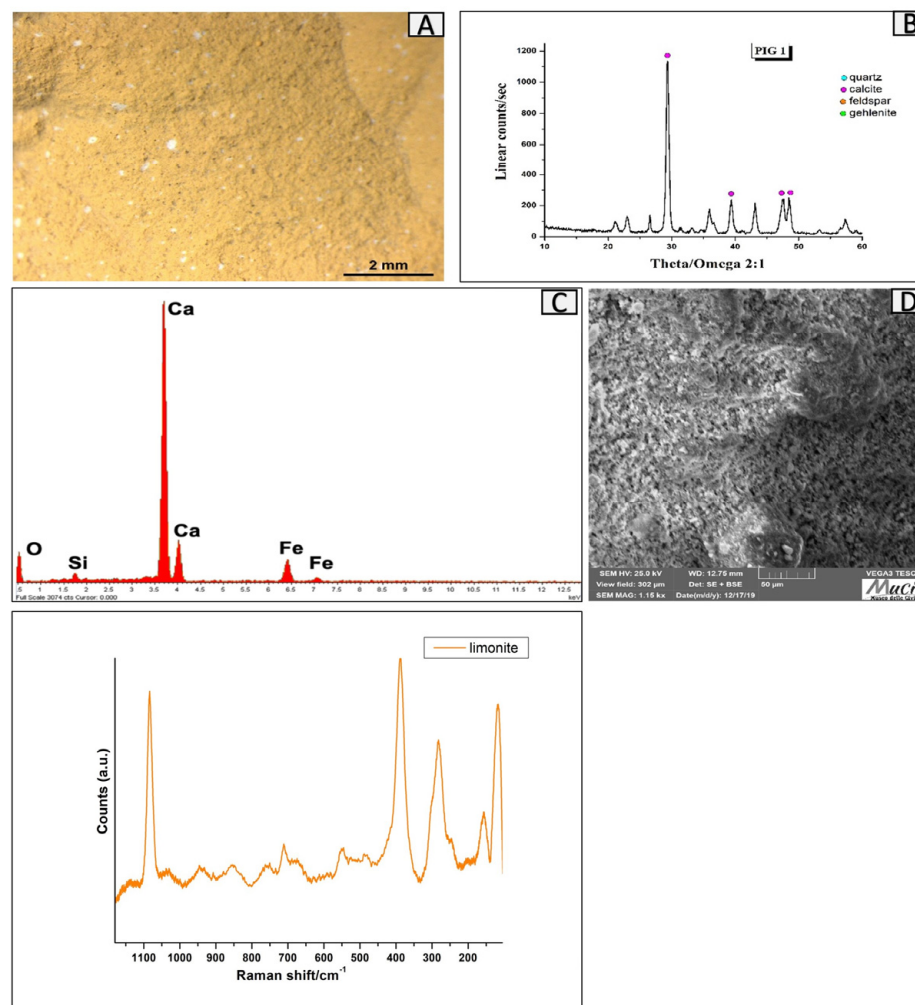


Figure 19. Surface area analysis of yellow clay, FIG1. (A) Optical and (D) backscattered SEM images of the clay. The XRD spectrum (B) identifies calcite (CaCO_3), quartz (SiO_2), feldspar (albite- $\text{NaAlSi}_3\text{O}_8$), and goethite ($\text{FeO}(\text{OH})$). The EDS area spectrum (C) reveals the presence of Ca, Fe, and Si. The μ -Raman spectrum (E) highlights the presence of limonite, ($\text{FeO}(\text{OH}) \cdot n\text{H}_2\text{O}$).

Table 7. EDS area analysis of the FIG1 clay fragment; * weight percentage (wt%), error $\pm 0.2\%$.

	O	Al	Si	Ca	Fe
FIG1 *	54.6	0.2	1	37.4	6.7

The colour is caused by limonite, ($\text{FeO}(\text{OH}) \cdot n\text{H}_2\text{O}$), as confirmed by the μ -Raman analysis. Yellow ochre is a natural pigment produced from clay containing limonite, whose colour can vary from light yellow to brownish yellow depending on the quantity and origin of the mineral. This pigment is different from Terra di Siena, whose colour is caused by missing manganese oxides. It was produced by finely grinding the clay, mixing it with water, and drying it at a low temperature to prevent colour change [22]. The numerous fragments of similar appearance that were found in the excavation area allowed us to hypothesise the presence of a place dedicated to the production of pigments.

The compact, reddish-orange clay fragment, C1A, was found in the furnace's quadrant A. The optical microscopical image (Figure 20A) shows a wrinkled surface with a variable grain size. The XRD spectrum (Figure 20B) identifies the presence of quartz (SiO_2), calcite (CaCO_3), and high albite ($\text{NaAlSi}_3\text{O}_8$). The SEM image (Figure 20D) confirms the heterogeneity of the clayey material's grain sizes. The EDS area analysis (Figure 20C, Table 8)

reveals high contents of Si (18.3%), Ca (10.8%), Al (6.1%), Ti, and Fe, elements often present in quartz clays.

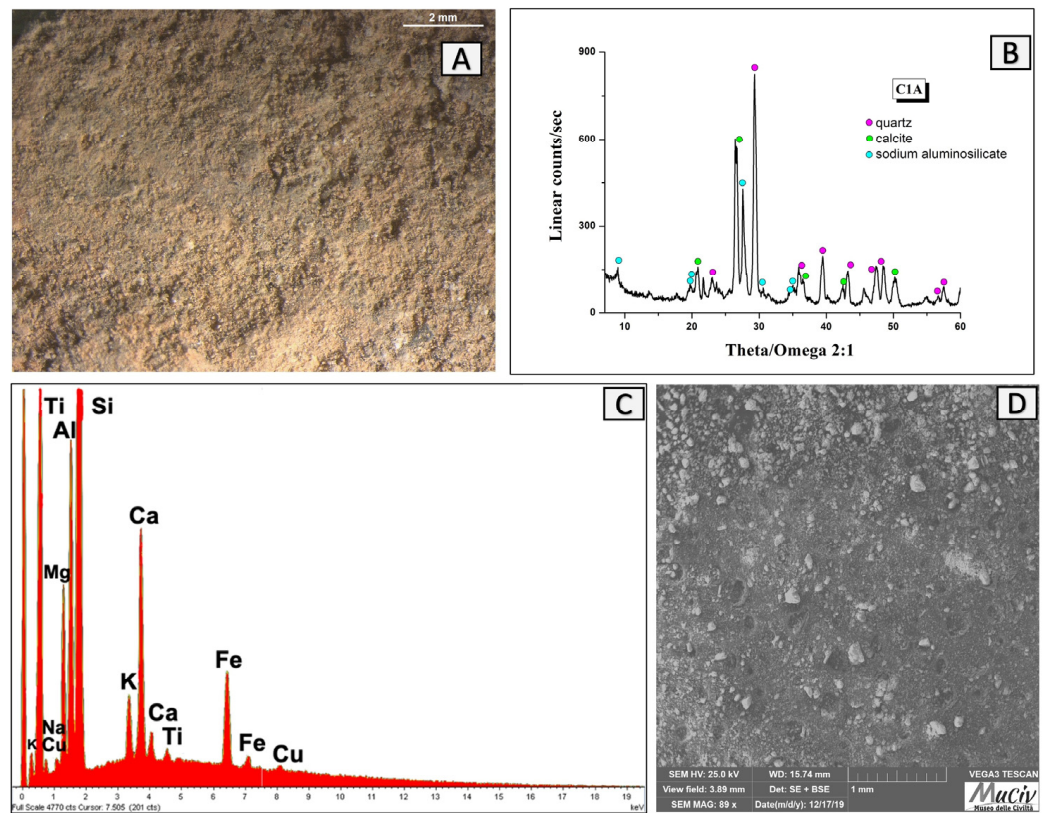


Figure 20. Surface area analysis of C1A fired clay. (A) Optical and (D) backscattered SEM images of fired clay. The XRD spectrum (B) reveals the mineralogical phases present: quartz (SiO_2), calcite (CaCO_3), and high albite ($\text{NaAlSi}_3\text{O}_8$). The EDS area analysis (C) revealed high contents of Si, Ca, and smaller amounts of Al, Ti, and Fe.

Table 8. EDS area analysis of the C1A clay fragment; * weight percentage (wt%), error $\pm 0.2\%$.

	O	Na	Mg	Al	Si	K	Ca	Ti	Fe	Cu
C1A *	56.5	0.4	1.7	6.1	18.3	3.4	10.8	0.2	2.1	0.2

The presence of high-temperature minerals, such as high albite, which crystallises at temperatures higher than $700\text{ }^\circ\text{C}$ and is stable up to roughly $900\text{ }^\circ\text{C}$, indicates that the material was subjected to heat treatments at medium temperatures. Since it is a very brittle material, it could not have been part of the furnace wall, but rather a refractory mortar, probably employed to bond the bricks of the heating surface.

The C1B clay fragment comes from quadrant A of the furnace. The clay observed using optical microscopy (Figure 21A) is characterised by a light yellow aspect. The mineralogical analysis (Figure 21B) shows the presence of calcite (CaCO_3), quartz (SiO_2), and high albite ($\text{NaAlSi}_3\text{O}_8$). The EDS analysis (Figure 21C, Table 9) detects a high amount of Ca (42.8%) and low concentrations of Si (3.5%) and Al (0.8%), while the morphology (SEM image, Figure 21D) highlights a crystalline structure.

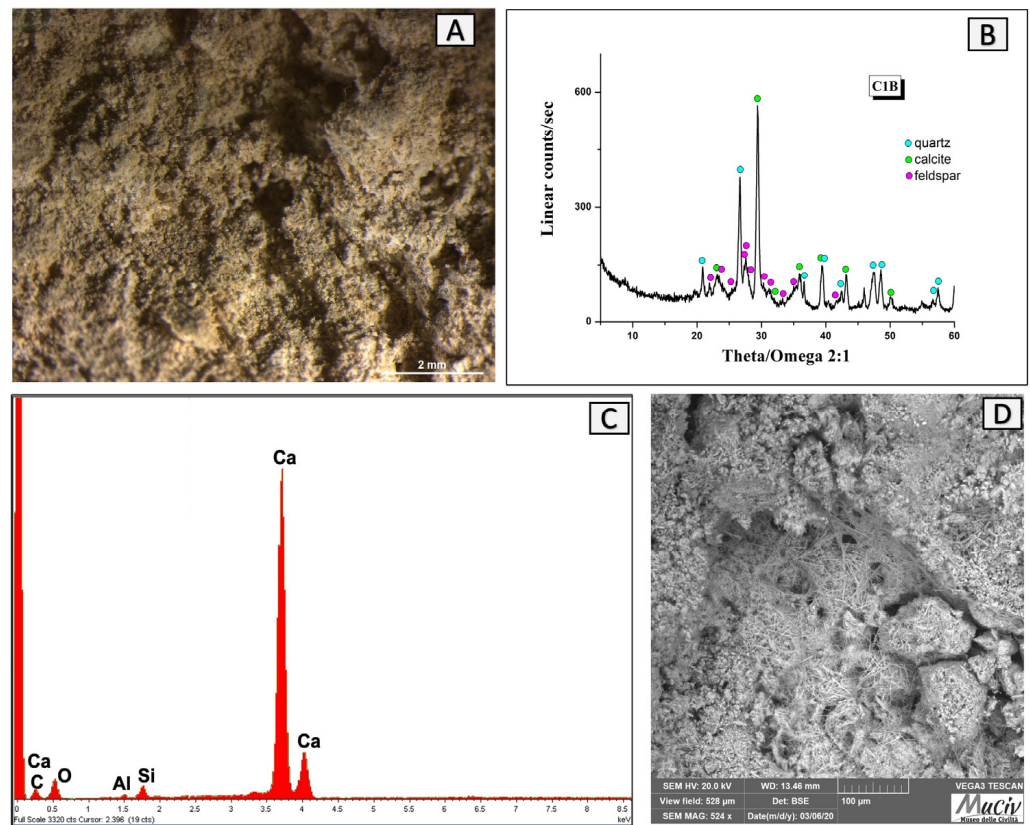


Figure 21. Surface area analysis of C1B fired clay. (A) Optical and (D) backscattered SEM images of fired clay. The XRD spectrum (B) reveals the mineralogical phases present: quartz (SiO₂), calcite (CaCO₃), and high albite (NaAlSiO₃). The EDS area analysis (C) detected a high amount of Ca and low concentrations of Si and Al.

Table 9. EDS area analysis of the C1B clay fragment; * weight percentage (wt%), error ± 0.2%.

	O	Mg	Al	Si	K	Ca	Fe
<i>C1B</i> *	51.5	0.2	0.8	3.5	0.2	42.8	0.6

The high calcium content suggests that the material © is the product of firing a calcareous clay at high temperatures (>800 °C), which induces the dissociation of calcite (CaCO₃) into calcium oxide (CaO) and carbon dioxide (CO₂). Because the volume of lime is significantly lower than that of carbonate, this change takes place with a large loss in volume. This transition, however, is reversible; in fact, after frying, the lime in the mixture can convert to calcite (carbonation), reacting with the CO₂ in the atmosphere [23]. Carbonation causes a rise in volume, which makes the material very brittle; this is a condition that occurs most often in calcareous clays. When the temperature rises above 900 °C, the lime bonds with the other elements of the clay to form silicates.

Fired calcareous clays are particularly hard and resistant but have a very high expansion coefficient. This reason leads us to rule out that this material belonged to the area of the furnace that was the most exposed to the heat, but it is possible that it was part of a structural section of the furnace with mechanical resistance properties [24].

The C2 clay fragment was found in quadrant A of the furnace and has a darker colour and a well-compacted structure compared to the other analysed clays. The optical image (Figure 22A) shows a compact and homogeneous morphology. The XRD analysis (Figure 22B) shows the presence of quartz (SiO₂), calcite (CaCO₃), high albite (NaAlSiO₃), and cristobalite (SiO₂). The area chemical analysis (Figure 22C, Table 10) detected the presence of Ca (12.6%), Si (23.6%), Al (1%), Fe (0.9%), and Mn (0.4%). The existence of large

hexagonal-shaped crystals highlighted in the SEM image (Figure 22D) indicates a heating process followed by slow cooling.

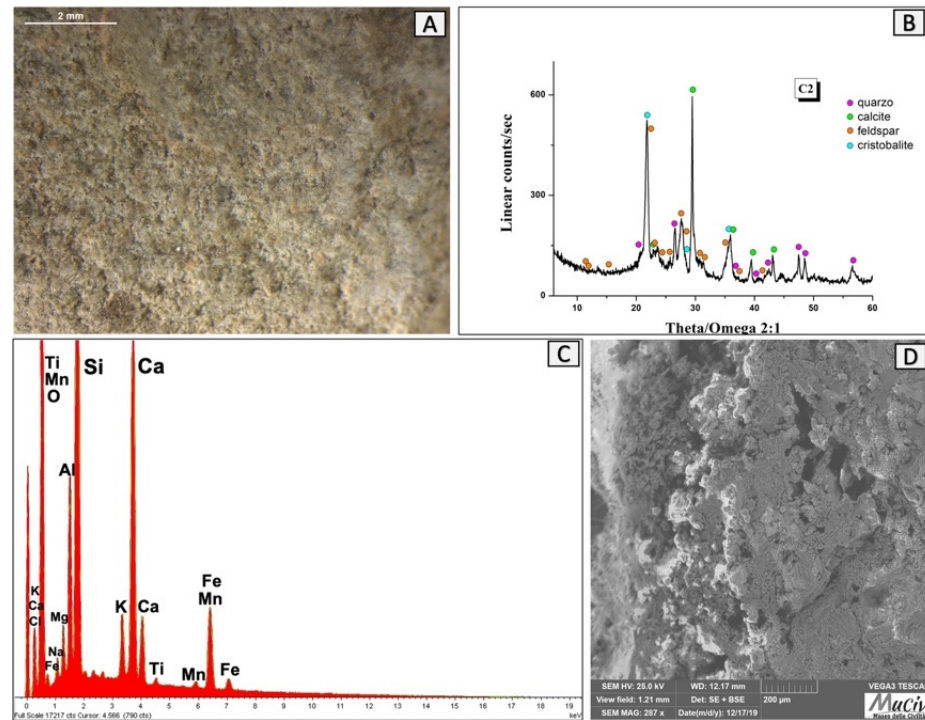


Figure 22. Surface area analysis of fired clay C2. (A) Optical and (D) backscattered SEM images of fired clay. The XRD spectrum (B) reveals the mineralogical phases present: quartz (SiO_2), calcite (CaCO_3), high albite ($\text{NaAlSi}_3\text{O}_8$), and hematite (Fe_2O_3). The EDS analysis (C) detected the presence of Ca, Si, Al, Fe, and Mn.

Table 10. EDS area analysis of the C2 clay fragment; * weight percentage (wt%), error $\pm 0.2\%$.

	O	Na	Mg	Al	Si	K	Ca	Mn	Fe
C2 *	60.5	0.2	0.2	1	23.6	0.4	12.6	0.4	0.9

The mineralogical analysis and the observed non-homogeneous colouration ranging from dark red to light grey reveal that the material was heated, reaching the calcite decomposition temperature ($800\text{ }^\circ\text{C}$), and the partial quartz transforms into cristobalite ($1100\text{ }^\circ\text{C}$), with raw light grey areas visible. In comparison to the C1B fired clay, it has lower carbonates and a greater amount of Si, rendering these materials more resistant and refractory. This material probably came from the furnace hob.

The C3 clay fragment was found in quadrant A of the furnace. The microscopy image (Figure 23A) reveals a homogeneous structure, similar to fragment C2 (Figure 22A), with lighter yellowish colours. μ -Raman spectroscopy (Figure 23B) detected the presence of quartz (SiO_2) and hematite (Fe_2O_3). The chemical analysis (Figure 23C, Table 11) detected the presence of Si (24.3%), Ca (12.3%), and Al (3.7%). The SEM image (Figure 23D) highlights a partial vitrification and a porosity of the material with the presence of evident crystalline structures. Based on these data, we may assume that it reached a temperature higher than $800\text{ }^\circ\text{C}$; the clay did not vitrify below this temperature.

This terracotta was probably part of the wall of the furnace, in an area where heat exposure was protracted.

The optical microscopical image of the SNZ1 clay fragment shows a compact, homogeneous, and light yellow clay (Figure 24A). μ -Raman spectroscopy (Figure 24B) highlighted the presence of goethite ($\text{FeO}(\text{OH})$). The chemical analysis (Figure 24C, Table 12) detected the presence of Ca (16.8%), Si (17.1%), Al (4.5%), and Fe (3.3%).

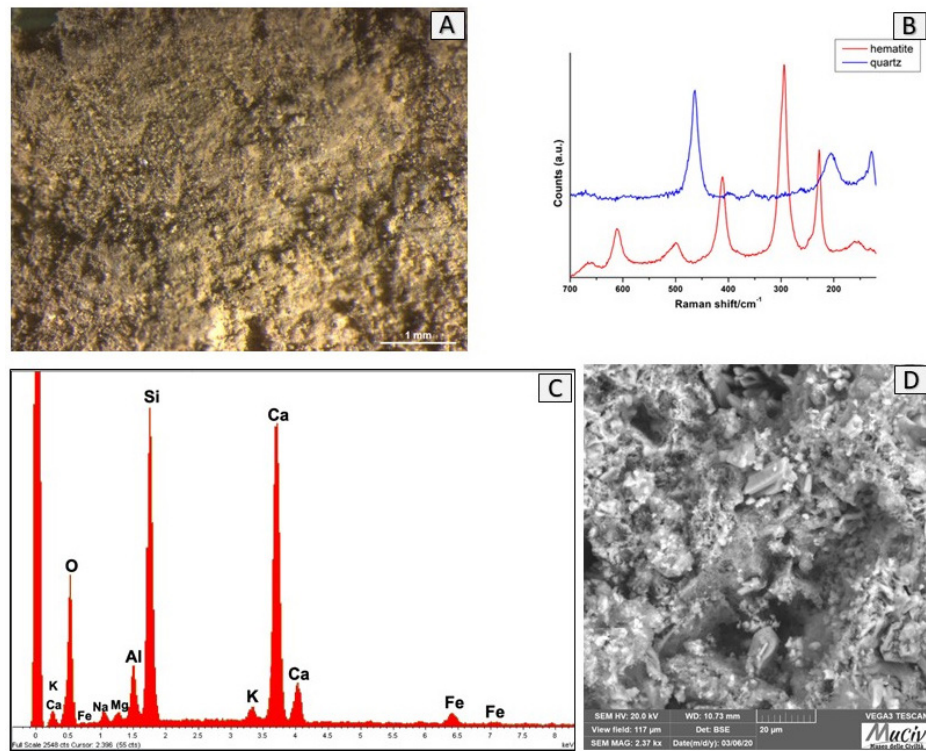


Figure 23. Surface analysis of C3 fired clay. (A) Optical and (D) backscattered SEM images of fired clay. The XRD spectrum (B) reveals the mineralogical phases present: quartz (SiO₂), goethite (FeO(OH)), and hematite (Fe₂O₃). The EDS area analysis (C) detected the presence of Si, Ca, and Al.

Table 11. EDS analysis of the C3 clay fragment; * weight per cent (wt%), error ± 0.2%.

	O	Na	Mg	Al	Si	K	Ca	Fe
C3 *	49	1.9	0.9	3.7	24.3	1.3	12.3	6.5

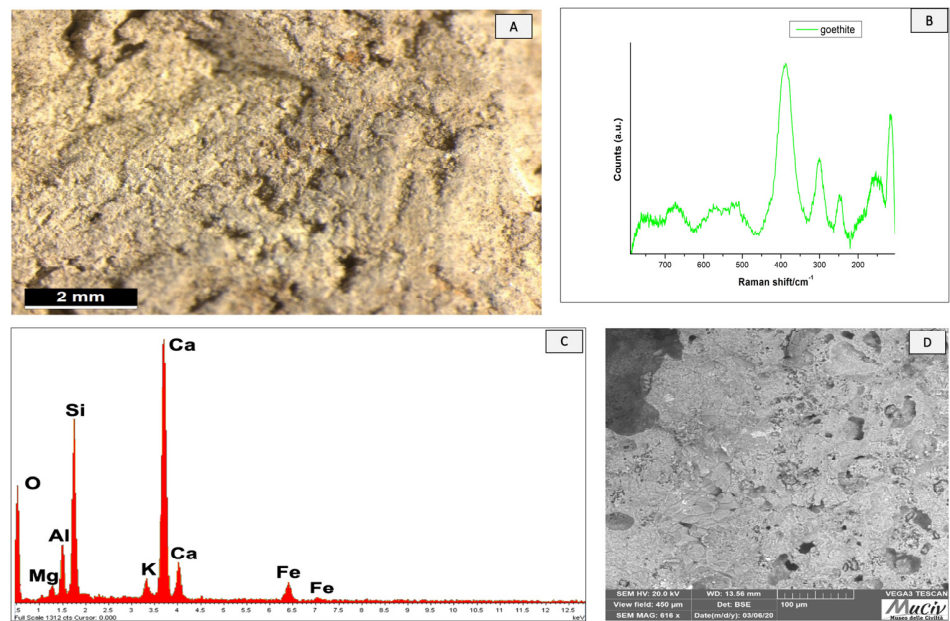


Figure 24. Surface analysis of SNZ1 fired clay. (A) Optical and (D) backscattered SEM images of fired clay. The Raman spectrum (B) reveals the presence of a goethite phase. The area chemical analysis (C) revealed the presence of Ca, Si, Al, and Fe.

Table 12. EDS area analysis of the SNZ1 clay fragment; * weight per cent (wt%), error $\pm 0.2\%$.

	O	Na	Mg	Al	Si	K	Ca	Ti	Fe
SNZ1 *	54.5	0.5	1.1	4.5	17.1	1.6	16.8	0.5	3.3

The SEM micrograph (Figure 24D) shows large crystals that were crystallised as a result of slower cooling and holes that were probably induced by thermal shocks at high temperatures. When observing the image, we also notice a porosity that could be associated with water loss during heating [25].

The results of the area chemical analyses reveal a quartz composition with calcite and traces of plagioclase, probably albite, and iron oxides. It is possible to deduce that the material was exposed to temperatures lower than those required for calcite decomposition.

3.3. Glassy Materials

The discovery of several glass fragments during the Palazzo Corsini excavation supports the possibility that glass artefacts were also produced in the furnace.

The INV1 glazed pottery was found in quadrant C. The optical image (Figure 25A) shows a shiny surface with a glassy nature and an olive green colour. The presence of quartz (SiO_2), calcite (CaCO_3), and apatite ($\text{Ca}_5(\text{PO}_4)_3[\text{F}, \text{OH}, \text{Cl}]$) is highlighted in the XRD spectrum (Figure 25B). A chemical analysis (Figure 25C, Table 13) detected the presence of elements characteristic of Roman glass, such as silicon, aluminium, and lead [26,27]. The SEM image (Figure 25D) highlights the artefact's superficial glassy layer, which can be identified by the typical conchoidal fracture. The term conchoidal refers to fractures having smooth, curving surfaces, which are typically found in quartz and glass [28].

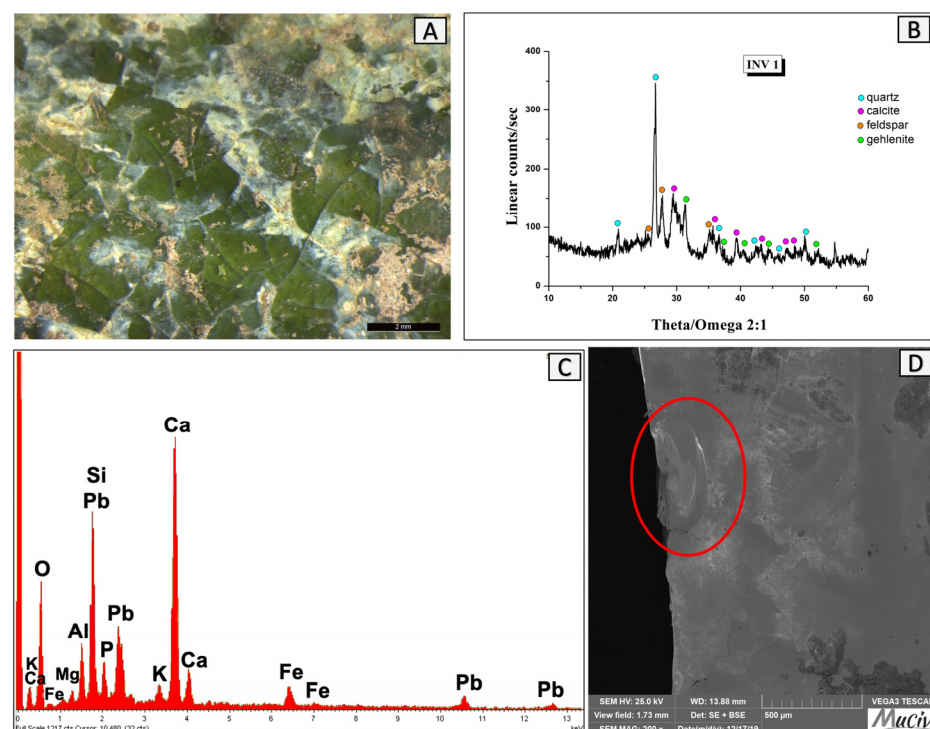
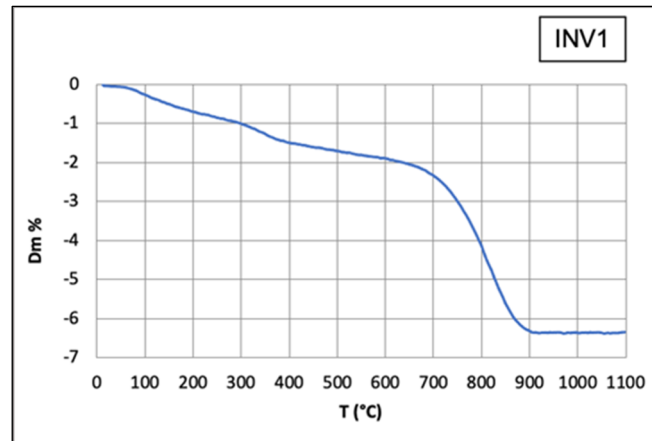


Figure 25. Surface analysis of INV1 glass. (A) Optical and (D) backscattered SEM images of the glass surface where the conchoidal breakage of the INV1 fragment can be observed (shown in the red circle). The XRD spectrum (B) reveals the mineralogical phases present: quartz (SiO_2), calcite (CaCO_3), and apatite ($\text{Ca}_5(\text{PO}_4)_3[\text{F}, \text{OH}, \text{Cl}]$). The area chemical analysis (C) detected the presence of Mg, Al, Si, P, K, Ca, Fe, and Pb.

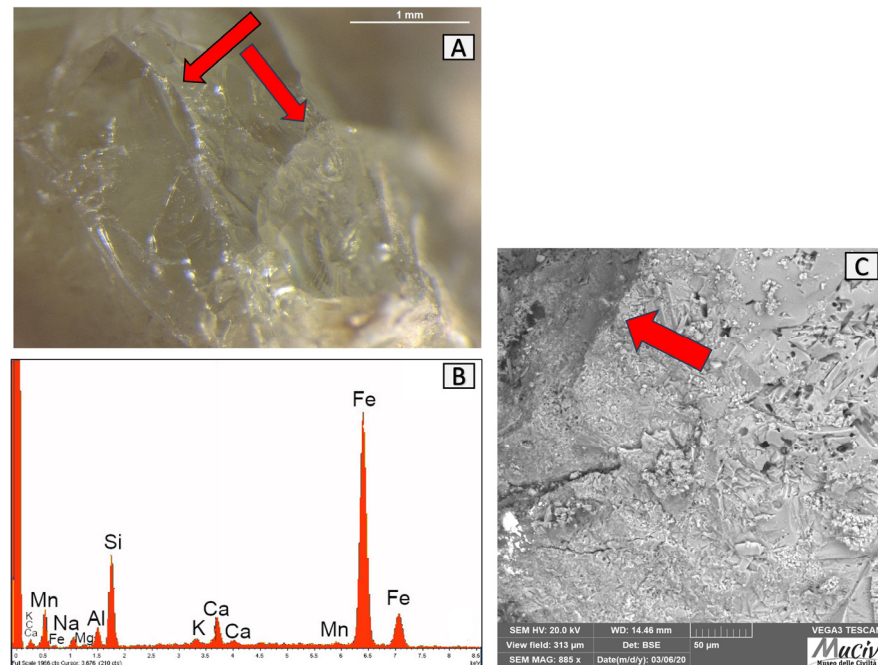
Table 13. EDS analysis of the INV1 fragment; * weight per cent (wt%), error $\pm 0.2\%$.

	MgO	Al ₂ O ₃	SiO ₂	P ₂ O ₅	K ₂ O	CaO	Fe ₂ O	PbO ₂
INV1 *	0.98	7.07	28.48	18.8	1.17	29.6	3.9	9.82

The TGA graph (Figure 26) shows a decrease from 750 °C to 850 °C due to the dissociation of CaCO₃.

**Figure 26.** TGA graph of the INV1 fragment shows a decrease from 750 °C to 850 °C due to the dissociation of CaCO₃.

Numerous frit fragments, including the FRT1 fragment investigated in this study, have been found between the vitreous materials discovered in quadrant C (Figure 27).

**Figure 27.** Surface analysis of FRT1 frit. (A) Optical and (C) backscattered SEM images where the conchoidal fracture structures of the FRT1 fragment are indicated by the red arrow. The EDS area analysis (B) detected the presence of Si, Na, Al, and K.

The frit is a powdered raw glass produced by calcining raw materials used to prepare paints and glazes, melting the components in refractory vessels (crucibles), and rapidly cooling the molten mass, for example, by throwing it into water [29]. The aim was to

transform a mass containing water-soluble raw materials into an insoluble glass in order to improve the uniformity of their distribution over the surfaces of the artefacts during processing. The translucent aspect of the colourless glass piece is highlighted through a microscopic examination (Figure 27A). The presence of Si, Na, Al, and K in the EDS area spectrum and chemical analyses (Figure 27B, Table 14) is typical of a glassy material. The SEM image (Figure 27C) shows a structure with conchoidal fractures characteristic of glass.

Table 14. EDS area analysis of the FRT1 fragment; * weight per cent (wt%), error $\pm 0.2\%$.

	Na ₂ O	MgO	Al ₂ O ₃	SiO ₂	K ₂ O	CaO	MnO	Fe ₂ O
<i>FRT1</i> *	3.6	0.7	5	25.1	1.1	15.1	0.3	49

The VET1 glass fragment was found in quadrant B. On the macroscopic level, we see a clear, colourless material with green reflections. The EDS spectrum and chemical analysis (Figure 28A, Table 15) revealed a high concentration of silicon oxide (77%) and traces of sodium oxide (0.7%) and aluminium oxide (5.6%). SEM microscopy (Figure 28B) allowed us to observe a conchoidal fracture structure (indicated by the arrow).

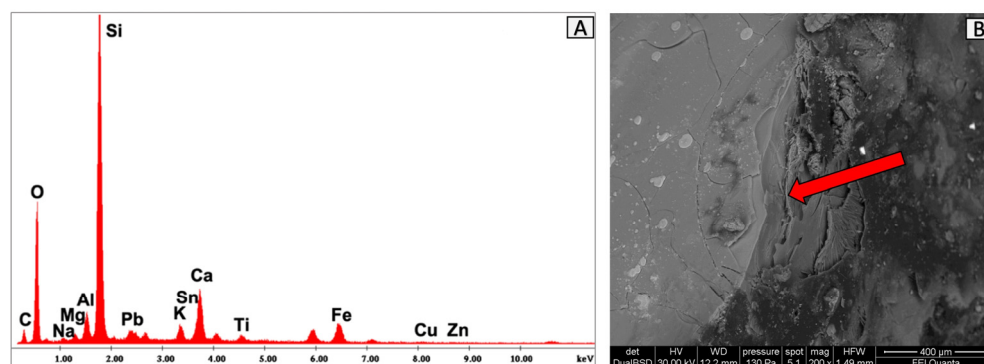


Figure 28. Surface analysis of VET1 glass. The EDS area analysis (A) detected the presence of silicon oxide and traces of sodium oxide and aluminium oxide. (B) Backscattered SEM image where the glass fractures of the VET1 fragment can be observed.

Table 15. EDS area analysis of the VET1 fragment; * weight per cent (wt%), error $\pm 0.2\%$.

	Na ₂ O	MgO	Al ₂ O ₃	SiO ₂	SnO ₂	K ₂ O	CaO	ZnO	Fe ₂ O	PbO ₂
<i>VET1</i> *	0.7	1.1	6	77	2	2.2	7.5	0.6	1.5	1

3.4. Bones Materials

Numerous processing wastes were also found in the excavation area, such as the OSS1 fragment found in quadrant C. The optical image (Figure 29A) and SEM image (Figure 29C) show the characteristic spongy structure of a bone. The presence of Ca and P comparable to hydroxyapatite ($\text{Ca}_{10}(\text{PO}_4)_6(\text{OH})_2$) is revealed by the EDS area spectrum (Figure 29B).

As previously mentioned, the microscopic investigations allowed us to observe an organic structure with porosities and cavities on the surface. These results, together with those of the chemical analysis, lead us to the conclusion that the OSS1 fragment belonged to a semi-finished bone product. Similarly, high concentrations of calcium and phosphorus were found in the VAS1 (Figure 16C) and INV1 (Table 13) glazed ceramic fragments, which suggests that bone fragments and/or dust were used to create the artefacts.

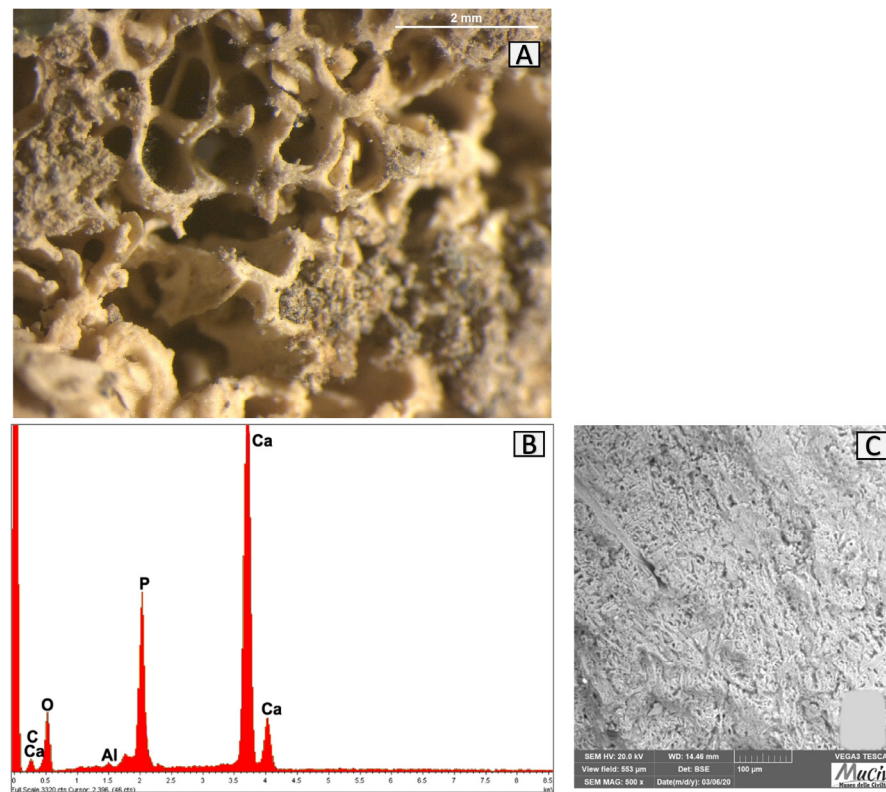


Figure 29. Surface analysis of OSS1 fragment. (A) Optical and (C) backscattered SEM images show the characteristic spongy structure of a bone. The EDS analysis (B) detected the presence of Ca and P comparable to the composition of hydroxyapatite ($\text{Ca}_{10}(\text{PO}_4)_6(\text{OH})_2$).

4. Discussion

The microscopic observations of the ceramic artefacts allowed the ceramics to be divided based on the morphology of the surfaces and the body. The light-coloured ceramics have a similar micro-morphology. The presence of calcite with a very fine grain size exposed to fire at no lower than 800 °C (producing calcium silico-aluminates) contributes to the bright appearances of the ceramics' surfaces [17,30].

In contrast, the ORL2 fragment (Figure 14A) presents a more zoned and grey colour, which could indicate a reducing–oxidising–reducing firing environment; in other words, the fragment may be from conditions that were not well controlled or from burial environments over the centuries. The pink colour of the VAS2 ceramics is due to the presence of Fe in the form of hematite and the high concentration of Ca, which reduces the reddening effect of iron oxides [31]. The ceramic bodies of the fragments are characterised by a CaO amount that is higher than 7–8%, which allows them to be included in the classification of calcareous ceramics [9].

From a mineralogical point of view, the analysis of the ceramic bodies mainly showed the presence of quartz, calcite, albite-feldspar, and gehlenite. This suggests that the clay utilised in the ceramic mixture is probably kaolinite. The mineral phases present in the ceramic body make it possible to estimate the firing temperature to which the artefact was subjected inside the furnace, as their formation depends on the temperature reached during the firing, the duration of the maximum peak, and the initial composition of the clay [32].

Therefore, the presence of gehlenite in all of the ceramic fragments revealed that temperatures higher than or equal to 850 °C were reached in the furnace, since gehlenite, as previously observed, is formed at $T > 800$ °C through a reaction among oxides of Al, Ca, and Si [33]. However, it is feasible that the firing temperature of the ceramics did not exceed 900/1000 °C, because cristobalite (SiO_2), which forms at temperatures higher than

1000 °C, is only present in fragment C2; as evidenced by Dapiaggi M. et al. [34], melting agents like Na and K could lower cristobalite's crystallisation temperature below 1000 °C.

Among minerals of high temperatures, such as anorthite and diopside, the presence of high albite ($\text{NaAlSi}_3\text{O}_8$), a sodium feldspar found in most pottery fragments that crystallises at temperatures above 700 °C and is stable up to 900 °C, has never been detected; this mineral provides additional support [30].

The presence of quartz in the ceramic mixture was most likely introduced to give the final product its refractory property. At the firing temperatures reached in the production of ancient ceramics, quartz maintains its crystalline properties, but at the same time, it participates in the formation reactions of other silicates. Finally, the CER1, ORL1, VAS1 and VAS2 fragments are similar, as they are composed of the same calcareous mixture including silicon and aluminium, revealing that the temperature of the furnace was similar for all products. During clay firing, the amount of calcium carbonate decreases with an increasing temperature, and most of what was observed in the XRD analyses is likely to indicate secondary formation, which means it forms as a result of reactions that occur in the ceramic mixture and is re-involved in the formation of new phases at temperatures above 900 °C. The TGA graphs support what is asserted, as the CER1 (Figure 12) and ORL2 (Figure 15) ceramics are comparable and show a weight loss from 750 °C to 900 °C, relative to calcite (CaCO_3), but there is no lattice water loss at lower temperatures. The analogies shown in the fragments lead us to believe, with a high degree of certainty, that they were produced in situ by utilising comparable clay, perhaps of local origin [19,35,36]. Furthermore, the ceramic fragments discovered in the Palazzo Corsini excavation have a fine and homogeneous grain size, indicating an accurate selection of the raw material: a clay with refined and careful characteristics.

The presence of iron oxides in all of the ceramic fragments indicates that they were fired in an oxidising environment [37,38].

Another significant feature, as previously mentioned, is the presence of calcium and phosphorus in the VAS1 ceramic. Given the abundance of bone materials discovered during the excavation, it may be hypothesised that the vase was used to contain bones (most likely of animal origin) or that the bone materials were used to produce ceramic objects.

The chemical compositions of the fired clay samples were compared with those of the ceramics taken on site. The concentrations of quartz and plagioclase, and in particular, calcite, in all of the clay fragments lead us to believe that these artefacts were not subjected to temperatures higher than 800 °C, as calcite decomposes above this temperature [39,40], although potentially, a minor concentration of calcite may form as a secondary product of lime carbonation. The absence of clay minerals in the fired clay indicates that it was heated at temperatures higher than 600 °C [41]. The presence of gehlenite in the ceramic fragments allows us to hypothesise that a processing temperature of more than 800–900 °C was used [33].

An optical analysis of the vitreous materials revealed similar structural properties, such as conchoidal fractures and translucent surfaces; these data can be attributed to a glass degradation called devitrification. Some variations appear in two fragments, FRT1 and VET1 (Figures 27 and 28), both from quadrant C, indicating a chromatic difference, most likely due to a different dosage of ingredients that cause the colour or a different production procedure.

The results of the chemical investigation of the INV1, FRT1, and VET1 fragments (Tables 13–15) shows glass-like elements (Si, Al, K, Na, and Ca) in comparable amounts. The examination of the distinctive elements (Si-Al-K) highlights that silicon-based materials should be used to produce glass materials. The low concentrations of K_2O (1.1–2.2%) and MgO (0.7–1.1%) in all fragments could indicate the use of natron ($\text{Na}_2\text{CO}_3 \cdot 10\text{H}_2\text{O}$), a sodium mineral (hydrated sodium carbonate) that was widely utilised as a flux throughout Europe from the first millennium BC to the ninth century AD [42] and used for artefacts during the Roman and early medieval periods [43]. The chemical analysis of the INV1 fragment (Figure 25C) highlighted high concentrations of CaO (29.6%), P_2O_5 (18.8%),

and PbO_2 (9.82%), which suggests the presence of apatite ($\text{Ca}_5(\text{PO}_4)_3 [\text{F}, \text{OH}, \text{Cl}]$). The stoichiometric ratio of Ca and P (2:1) made it possible to assume the presence of an organic material in the fragment, such as bone dust. The hypotheses formulated on the use of this organic material are different: One hypothesis is the use of bone powder as an economical glass opacifier, a system used in the Middle Ages for the production of glazes, that was fired by adding cassiterite (SnO_2), a mineral that was not found in the fragment under examination. Another theory connects the presence of bone dust (apatite) to the process of lead extraction [44].

Furthermore, based on the results of the analyses, it was possible to establish that the firing temperature for all of the vitreous fragments should be about 800 °C, as the vitrification of the material was not possible at lower temperatures [45,46].

The microscopic investigations allowed us to observe an organic structure of bone materials with porosities and cavities on the surface. These results, together with those of the chemical analysis, lead us to the conclusion that the OSS1 fragment belonged to a semi-finished bone product. Similarly, high concentrations of calcium and phosphorus were found in the VAS1 (Figure 16C) and INV1 (Table 13) glazed ceramic fragments, which suggests that bone fragments and/or dust were used to create the artefacts.

In the excavation of Villa Corsini, the discovery of both the remains of structures similar to kilns and the large quantity and variety of ceramic fragments that have come to light, in addition to the presence of canalisations intended for the drainage of water coming from the Janiculum, appears to confirm the hypothesis of the conversion of at least part of the urbanised area to a productive area.

Moreover, the data allow us to assume that the production of the analysed ceramic samples took place on site using a type of kaolinitic raw clay from local areas, with small differences in processing.

Another interesting piece of information is provided by the presence of traces of vitrification on the surfaces of the ceramics and by the discovery of fragments of glazed ceramics, indicating that the furnace of Palazzo Corsini had also been used for the creation of glazes on ceramics intended for domestic and industrial uses.

Together with the pottery materials mentioned above, other finds such as pigments and bone pieces were discovered in the same area. The discovery of a large number of pigments leads us to believe that we are in the presence of a workshop that is specialised not only in the production of ceramics but also in the processing of pigments for commercial use.

The presence of bone tools and animal bone fragments suggests their employment in the processing of clay mixtures, a practice known in the production of ancient vases, particularly to improve the brilliance of the surfaces, without ruling out the possibility of the on-site processing of bone artefacts.

5. Conclusions

The aim of this investigation was to analyse the materials and structures discovered during the excavation by examining the archaeological complex of the archaeological area situated in the garden of Palazzo Corsini. This study allowed us to determine potential relationships between the scientific data from the archaeometric analyses conducted on the chosen materials and the historical–archaeological data obtained from the study of the archaeological finds (excavation data, typology of artefacts, etc.).

The investigation data gave us information about the artefacts' technological history, particularly about the source of materials, production aspects, and their possible uses.

The structure that emerged in quadrant A most likely belonged to a Roman-era furnace intended for the production of different types of materials, likely active between the first century AD and the third century AD. This result was confirmed by the archaeological data without excluding its use even in late antiquity, as the discovery of some finds with later dates would seem to confirm.

The results confirmed the hypothesis that there was an industrial production area in the region located between the slopes of the Janiculum to the west and the Tiber, with a big complex of workshops distributed in several areas for a variety of production processes.

Although many furnaces from the Roman era have been discovered in the Lazio area, most of which were used for the production of bricks with only a small portion of ceramic artefacts, the particularity of the structure discovered in the excavation of Palazzo Corsini consists of several kinds of productions regarding the same type of place and intended use, as well as its topographical location near the walls of the city, resulting in an urban context. Further archaeometrical and archaeological research is needed to confirm the developed hypothesis.

Author Contributions: Conceptualisation, T.d.C.; methodology, T.d.C., P.F., F.S. and R.S.; validation, T.d.C., S.B., F.S. and A.M.; formal analysis, S.B. and T.d.C.; investigation, S.B. and T.d.C.; resources, P.F. and R.S.; data curation, T.d.C., A.M. and F.S.; writing—original draft preparation, T.d.C.; writing—review and editing, T.d.C., A.M., V.R., F.S., P.F., R.S. and S.B.; visualisation, V.R.; supervision, T.d.C. All authors have read and agreed to the published version of the manuscript.

Funding: This research received no external funding.

Data Availability Statement: The data presented in this study are available in this article.

Acknowledgments: The authors acknowledge Claudio Veroli (ISMN-CNR) for providing skilful XRD technical assistance, Bruno Brunetti for helping with the TG analysis, and Daniela Ferro for her involvement in a helpful SEM discussion.

Conflicts of Interest: Author Simone Bruno was employed by the company Deloitte Nexthub S.r.l S.B, The remaining authors declare that the research was conducted in the absence of any commercial or financial relationships that could be construed as a potential conflict of interest.

References

- Borsellino, E. *Palazzo Corsini*; Istituto Poligrafico e Zecca dello Stato: Roma, Italy, 2002; pp. 38–60. ISBN 10: 8824035728.
- Fabbri, M.; Lanzini, M.; Manicella, D.; Succhiarelli, C. *I Geositi del Territorio di Roma Capitale*; Società italiana di Geologia Ambientale: Roma, Italy, 2014; pp. 34–48.
- Corazza, A.; Lombardi, L. Le sorgenti storiche di Roma. *Acque Sotter. Ital. J. Groundw.* **2015**, *4*, 71–73. [\[CrossRef\]](#)
- Maritan, L.; Mazzoli, C.; Dal Sasso, G.; Mazzocchin, S.; Cipriano, S. Archaeometric study on the ceramic production of the Roman Time potters' quarter of via Montona in Padua, Italy: From the reference groups to the regional distribution of coarse and fine ware. *Eur. Phys. J. Plus* **2018**, *133*, 358. [\[CrossRef\]](#)
- Balducci, L.A. La cronologia di officine urbane di lucerne: Contesto ostiense di età antonina. In *Actes de la VIIe Rencontre Franco-Italienne sur L'épigraphie du Monde Romain, Proceedings of the Rome: École Française de Rome, Rome, Italy, 5–6 June 1992*; École Française de Rome: Rome, Italy, 1992; pp. 447–448. ISBN 2-7283-0302-9.
- Freestone, I. *Handbook of Archaeological Sciences*; John Wiley & Sons Ltd.: Chichester, UK, 2023; pp. 615–627. ISBN 9781119592044.
- Pallecchi, S. *Materiali per Populonia 7*; ETS Edizioni: Pisa, Italy, 2008; pp. 323–328. ISBN 9788846721778.
- González Tobar, I. Trends in the production of olive oil amphorae at ceramic workshops in Roman Baetica: A chrono-proportional representation method. *Antiquity* **2023**, *97*, 927–944. [\[CrossRef\]](#)
- Cuomo Di Caprio, N. *Ceramica in Archeologia 2, Antiche Tecniche di Lavorazione e Moderni Metodi di Indagine*; ERMA di Bretschneider: Roma, Italy, 2007; pp. 47–95. ISBN 9788882653972.
- Guerrini, C.; Mancini, L. *Introduzione Allo Studio Della Ceramica in Archeologia*; Centro Editoriale Toscano sas: Florence, Italy, 2007; pp. 155–163. ISBN 10: 88-7957-269-5.
- Rossi, M.; De Riso, N.; Caterino, M.; Ferraro, G.; Cicala, L.; Ferrara, B.; Gassner, V.; Vergara, A. On the productive function of furnaces in archaeological sites. *J. Raman Spectrosc.* **2020**, *52*, 217–229. [\[CrossRef\]](#)
- Rieger, A.K.; Möller, H. Kilns, Commodities and Consumers: Greco-Roman Pottery Production in Eastern Marmarica (Northwestern Egypt). *Archäologischer Anz.* **2011**, *1*, 141–170. [\[CrossRef\]](#)
- Morandi, L.F.; Amicone, S. Ceramic traditions and technological choices revealed by early Iron Age vessels: The case of Vetulonia (southern Tuscany). *STAR Sci. Technol. Archaeol. Res.* **2023**, *9*, 2217558. [\[CrossRef\]](#)
- Pena, J.T. *Roman Pottery in the Archaeological Record*; Cambridge University Press: Cambridge, UK, 2007; ISBN 9780511499685.
- Rye, O.S. *Pottery Technology: Principles and Reconstruction*; Taraxum: Washington, DC, USA, 1981.
- Cosentino, D.; Cipollari, P.; Di Bella, L.; Esposito, A.; Faranda, C.; Funicello, R.; Giordano, G.; Gliozzi, E.; Mattei, M.; Mazzini, I.; et al. Geologia dei monti della Farnesina (Roma): Nuovi dati di sottosuolo dalla galleria Giovanni XXII. *Mem. Descr. Della Carta Geol. D'Italia* **2008**, *80*, 285–313.

17. Drebuschak, V.; Mylnikova, L.; Drebuschak, T.; Boldyrev, V. The investigation of ancient pottery: Application of thermal analysis. *J. Therm. Anal. Calorim.* **2005**, *82*, 617–626. [[CrossRef](#)]
18. Pérez-Monserrat, E.M.; Maritan, L.; Baratella, V.; Vidale, M. Production Technologies and Provenance of Ceramic Materials from the Earliest Foundry of Pre-Roman Padua, NE Italy. *Heritage* **2023**, *6*, 2956–2977. [[CrossRef](#)]
19. Drebuschak, V.A.; Mylnikova, L.N.; Molodin, V.I. Thermogravimetric investigation of ancient ceramics. *J. Therm. Anal. Calorim.* **2007**, *90*, 73–79. [[CrossRef](#)]
20. Ceccarelli, L.; Bellotto, M.; Caruso, M.; Cristiani, C.; Dotelli, G.; Gallo Stampino, P.; Gasti, G.; Primavesi, L. Characterization of clays and the technology of Roman ceramics production. *Clay Miner.* **2018**, *53*, 413–429. [[CrossRef](#)]
21. Kresten, P.; Berggren, G. The thermal decomposition of vermiculite. *Thermochim. Acta* **1978**, *23*, 171–182. [[CrossRef](#)]
22. Fioretti, G.; Clausi, M.; Eramo, G.; Longo, E.; Monno, A.; Pinto, D.; Tempesta, G. Non-Invasive and Sustainable Characterization of Pigments in Wall Paintings: A Library of Apulian Colors. *Heritage* **2023**, *6*, 1567–1593. [[CrossRef](#)]
23. Karunadasa, K.S.P.; Manoratne, C.H.; Pitawala, H.M.T.G.A.; Rajapakse, R.M.G. Thermal decomposition of calcium carbonate (calcite polymorph) as examined by in-situ high-temperature X-ray powder diffraction. *J. Phys. Chem. Solids* **2019**, *134*, 21–28. [[CrossRef](#)]
24. Borgers, B.; Tol, G.; de Haas, T. Reconstructing production technology and distribution, using thin section petrography: A pilot study of Roman pottery production in the Pontine region, Central Italy. *J. Archaeol. Sci. Rep.* **2018**, *21*, 1064–1072. [[CrossRef](#)]
25. Matarazzo, T.; Berna, F.; Goldberg, P. Micromorphological study of concotto surface protected by Avellino eruption in 3945 ± 10 cal. BP at the Early Bronze Age of Afragola village in southern Italy. *Environmental. Archaeol.* **2017**, *22*, 365–380. [[CrossRef](#)]
26. Maccabruni, C. *Céramiques Hellénistiques et Romaines*; Université de Franche-Comté: Besançon, France, 1987; pp. 167–190.
27. Sastri, S.C.; Sauvage, T.; Wendling, O.; Bellamy, A.; Humburg, C. Smoky Wood-Fired Ancient Glass Furnaces: Carbon Analysis of Roman Glass by 2.0 MeV Deuteron Activation Technique. *Minerals* **2023**, *13*, 1001. [[CrossRef](#)]
28. Witthoft, J. The mechanics of conchoidal fracture: A bibliographic note. *News. Lithic Technol.* **1974**, *3*, 50–53.
29. Silvestri, A.; Molin, G.; Salviulo, G. Roman and Medieval glass from the Italian area: Bulk characterization and relationships with production technologies. *Archaeometry* **2005**, *47*, 797–816. [[CrossRef](#)]
30. Schomburg, J. Thermal reactions of clay minerals: Their significance as “archaeological thermometers” in ancient potteries. *Appl. Clay Sci.* **1991**, *6*, 215–220. [[CrossRef](#)]
31. Wang, S.; Gainey, L.; Mackinnon, I.D.R.; Xi, Y. High- and low-defect kaolinite for brick making: Comparisons of technological properties, phase evolution and microstructure. *Constr. Build Mater.* **2023**, *366*, 130250. [[CrossRef](#)]
32. de Caro, T.; Riccucci, C.; Parisi, E.I.; Renzulli, A.; Del Moro, S.; Santi, P.; Faraldi, F. Archaeo-metallurgical studies of tuyeres and smelting slags found at Tharros (north-western Sardinia, Italy). *Appl. Phys. A Mater.* **2013**, *11*, 933–943. [[CrossRef](#)]
33. Traoré, K.; Kabré, T.S.; Blanchart, P. Gehlenite and anorthite crystallisation from kaolinite and calcite mix. *Ceram. Int.* **2003**, *29*, 377–383. [[CrossRef](#)]
34. Dapiaggi, M.; Pagliari, P.; Pavese, A.; Sciascia, L.; Merli, M.; Francescon, F. The formation of silica high temperature polymorphs from quartz: Influence of grain size and mineralising agents. *J. Eur. Ceram. Soc.* **2015**, *16*, 4547–4555. [[CrossRef](#)]
35. Borgers, B.; Ionescu, C.; Willems, S.; Barbu-Tudoran, L.; Bernroider, M.; Clotuche, R. Continuity and diversity of Roman pottery production at Famars (northern France) in the 2nd–4th centuries AD: Insights from the wasters. *Archaeol. Anthropol. Sci.* **2020**, *12*, 221. [[CrossRef](#)]
36. Brown, A.E.; Sheldon, H.L. *The Roman Pottery Manufacturing Site in Highgate Wood: Excavations 1966–1978*; Archaeopress: Oxford, UK, 2018; ISBN 978-1-78491-978-8.
37. Borgers, B.; Willems, S.; Dupuis, C.; Clotuche, R. Technological knowledge and transfer of Roman pottery production in Civitas Nerviorum (northern France, central Belgium) during the 1st–3rd centuries CE. *J. Archaeol. Sci. Rep.* **2021**, *38*, 103061. [[CrossRef](#)]
38. El Halim, M.; Daoudi, L.; El Ouahabi, M.; Rousseau, V.; Cools, C.; Fagel, N. Mineralogical and geochemical characterization of archaeological ceramics from the 16th century El Badi Palace, Morocco. *Clay Miner.* **2018**, *53*, 459–470. [[CrossRef](#)]
39. Cultrone, G.; Rodriguez-Navarro, C.; Sebastian, E.; Cazalla, O.; De La Torre, M.J. Carbonate and silicate phase reactions during ceramic firing. *Eur. J. Mineral.* **2001**, *13*, 621–634. [[CrossRef](#)]
40. Lesigarski, D.; Jordanova, N.; Kostadinova-Avramova, M.; Bozhinova, E. Clay source and firing temperatures of Roman ceramics: A case study from Plovdiv, Bulgaria. *Geoarchaeology* **2020**, *35*, 287–309. [[CrossRef](#)]
41. Di Maio, G.; Balassone, G.; Ferrow, E.; Barca, D.; Mormone, A.; Petti, C.; Mondillo, N. Mineralogical and geochemical characterization of the concotto artefacts from firing places of Longola protohistoric settlement (Naples). *Period. Mineral.* **2013**, *80*, 353–358. [[CrossRef](#)]
42. Mirti, P.; Lepora, A.; Sagui, L. Scientific analysis of seventh-century glass fragments from the Crypta Balbi in Rome. *Archaeometry* **2000**, *42*, 359–374. [[CrossRef](#)]
43. Gallo, F.; Marcante, A.; Silvestri, A.; Molin, G.; Degryse, P.; Ganio, M. I vetri della casa delle bestie ferite ad Aquileia: Uno studio archeologico e archeometrico. In *L’architettura Privata ad Aquileia in età Romana, Proceedings of the Edilizia Domestica ad Aquileia e nel Suo Territorio, Padova, Italy, 21–22 February 2011*; Padova University Press: Padova, Italy, 2011; pp. 355–369. ISBN 978-88-9738-519-6.
44. Briano, A. Indagini archeometriche preliminari sulle invetriate in monocottura dal castello di Donoratico (LI). In *Storie di Ceramica 4 -Ceramica e Archeometria-*, *Proceedings of the Storie di Ceramiche, Pisa, Italy, 10 June 2017*; All’Insegna del Giglio s.a.s.: Sesto Fiorentino (FI), Italy, 2018; pp. 30–33. ISBN 978-88-7814-875-8.

-
45. Giorgetti, D. *Le Fornaci Romane di Alcamo*; ARACNE: Roma, Italy, 2006; pp. 11–35. ISBN 88-548-0596-3.
 46. Gentelli, L.; Medhat, A.R. A multi-analytical approach for the archaeometric identification of a Roman period glass furnace in the central Nile delta. *J. Archaeol. Sci. Rep.* **2017**, *11*, 330–337. [[CrossRef](#)]

Disclaimer/Publisher’s Note: The statements, opinions and data contained in all publications are solely those of the individual author(s) and contributor(s) and not of MDPI and/or the editor(s). MDPI and/or the editor(s) disclaim responsibility for any injury to people or property resulting from any ideas, methods, instructions or products referred to in the content.